



Evaluating isoprenoidal hydroxylated GDGT-based temperature proxies in surface sediments from the global ocean

Devika Varma^{a,*}, Ellen C. Hopmans^a, Zoë R. van Kemenade^a, Stephanie Kusch^b, Sonja Berg^c, Nicole J. Bale^a, Francesca Sangiorgi^d, Gert-Jan Reichart^{a,d}, Jaap S. Sinninghe Damsté^{a,d}, Stefan Schouten^{a,d}

^a NIOZ Royal Netherlands Institute for Sea Research, Landsdiep 4, 1797 SZ 't Horntje, Texel, The Netherlands

^b ISMER Institute of Marine Sciences, University of Quebec Rimouski, Rimouski, QC G5L 3A1, Canada

^c Institute of Geology and Mineralogy, University of Cologne, Zùlpicher Str. 49b, 50674 Cologne, Germany

^d Department of Earth Sciences, Utrecht University, Princetonlaan 8a, 3584 CB Utrecht, The Netherlands

ARTICLE INFO

Associate editor: Shucheng Xie

Keywords:

Hydroxylated GDGTs

TEX₈₆

RI-OH

%OH

Surface sediments

ABSTRACT

Recently developed temperature proxies based on hydroxylated isoprenoid Glycerol Dialkyl Glycerol Tetraethers (OH-isoGDGTs), such as %OH, RI-OH, RI-OH' and OH^C, have shown potential for reconstructing past temperature changes. However, progress has been limited by the lack of a global core-top calibration with ample geographical coverage. Here, we compile an extensive global surface sediment dataset of OH-isoGDGTs as well as regular isoprenoid GDGTs (isoGDGTs), with both data generated at NIOZ (n = 575) and previously published data from other laboratories (n = 297). We find interlaboratory differences for proxy indices that incorporate both OH-isoGDGTs and regular isoGDGTs, indicating that care must be taken in compiling large GDGT datasets from multiple laboratories. Our results confirm a strong temperature signal in the isoGDGT distribution, especially for OH-isoGDGT-0 and non-hydroxylated isoGDGTs, but also reveal that water depth might have an impact on the distribution of OH-isoGDGTs with 1 and 2 cyclopentane moieties. This will affect the RI-OH and RI-OH' indices, particularly in tropical regions, where OH-isoGDGT-0 occurs at low abundance. We explore new proxy indices that combine the temperature dependence of both isoGDGT and OH-isoGDGT distributions and propose the use of TEX₈₆^{OH}, which includes OH-isoGDGT-0 in the denominator of the TEX₈₆ index. This modification leads to a much higher temperature sensitivity of the index, especially in regions with annual mean sea surface temperatures between 5 and 15 °C. Application of this novel paleothermometer to a polar sediment core suggests that this proxy is likely to result in more reliable temperature reconstructions in polar regions where OH-isoGDGTs are abundant.

1. Introduction

Biomarker lipids produced by microorganisms are an important tool for the reconstruction of past sea (sub)surface temperatures, which plays a significant role in understanding Earth's climate history and modelling future climate. One of the most commonly used biomarker proxies for studying past temperature change is the U₃₇^K index based on alkenones (Prahl and Wakeham, 1987). Alkenones are molecules produced by some species of haptophyte algae (de Leeuw et al., 1980; Volkman et al., 1980), where the degree of unsaturation changes with growth temperature (Brassell et al., 1986; Prahl and Wakeham, 1987). However,

alkenones are rarely found in sediments older than 50 Ma (Brassell, 2014) and cannot be used for temperature reconstructions above ~ 29 °C (e.g. Müller et al., 1998). Another frequently used organic seawater temperature proxy is the TEX₈₆ (TetraEther indeX of 86 carbons; Schouten et al., 2002) based on the relative abundance of isoprenoidal glycerol dialkyl glycerol tetraether lipids (isoGDGTs) with 1 to 3 cyclopentane moieties and the crenarchaeol isomer (see Table 1 for the definition of all isoGDGT-based proxies), which contains an additional cyclohexane moiety (Sinninghe Damsté et al., 2002; Holzheimer et al., 2021). These isoGDGTs are predominantly produced in the ocean by a group of archaea (Sinninghe Damsté et al., 2002; Schouten et al., 2013b; Zeng et al., 2019), i.e., Thaumarchaeota (named *Nitrososphaeria* in the

* Corresponding author.

E-mail address: devika.varma@nioz.nl (D. Varma).

<https://doi.org/10.1016/j.gca.2023.12.019>

Received 25 October 2023; Accepted 15 December 2023

Available online 18 December 2023

0016-7037/© 2023 The Authors. Published by Elsevier Ltd. This is an open access article under the CC BY license (<http://creativecommons.org/licenses/by/4.0/>).

Global Taxonomy Database; Rinke et al., 2021), which are widespread in the global ocean and oxidize ammonium (e.g. Karner et al., 2001a; Sinninghe Damsté et al., 2002; Könneke et al., 2005; Schouten et al., 2013b; Zeng et al., 2019). At higher growth temperatures, they increase the number of cyclopentane moieties in their core membrane GDGTs (Gabriel and Chong, 2000; Wuchter et al., 2004; Elling et al., 2015), forming the basis for the definition, calibration, and successful application of the TEX₈₆ palaeothermometer (Schouten et al., 2002, 2013b). However, correlation of TEX₈₆ in surface sediments with annual mean sea (sub)surface water temperatures shows major scatter and potentially non-linear relationships (cf. Kim et al., 2010; Schouten et al., 2013b; Tierney and Tingley, 2014, 2015). This is likely predominantly caused by varying contributions of phylogenetically different groups of Thaumarchaeota inhabiting different water depths (Kim et al., 2015; Villanueva et al., 2015; Zhu et al., 2016; Besseling et al., 2019) and impact of nutrient conditions (Elling et al., 2015; Hurley et al., 2016; Evans et al., 2019), complicating the application of TEX₈₆ as a seawater temperature proxy (e.g. Huguet et al., 2007; Ho and Laepple, 2016; Hurley et al., 2018; Zhang and Liu, 2018). The TEX₈₆-temperature relationship flattens below ~ 12 °C, which restricts the use of this proxy in cold polar regions (cf. Kim et al., 2010). Accordingly, the TEX₈₆^L index, which excludes the crenarchaeol isomer completely and isoGDGT-3 from the numerator of the originally defined TEX₈₆ index (Table 1), has been

suggested as an alternative temperature proxy for temperatures < 15 °C (Kim et al., 2010). However, TEX₈₆^L is strongly impacted by the export of isoGDGTs from thaumarchaeotal communities that inhabit different water depths (e.g. Inglis et al., 2015; O'Brien et al., 2017) and have different isoGDGT [2]/[3] ratios (Taylor et al., 2013; Villanueva et al., 2015; Kim et al., 2016; Besseling et al., 2019; Rattanasriampaipong et al., 2022). Hence, TEX₈₆^L-based temperature reconstructions need to be applied with caution (cf. Taylor et al., 2013; Ho et al., 2014; Inglis et al., 2015).

More recently, paleothermometers based on hydroxylated isoGDGTs (OH-isoGDGTs) have been developed. OH-isoGDGTs containing one or two hydroxy groups attached to their biphytanyl chains were first identified by Liu et al., (2012a) in a marine sediment. Huguet et al. (2013) showed that OH-isoGDGTs are ubiquitous in marine and freshwater systems. Moreover, OH-isoGDGTs were also identified in soils (Kang et al., 2017; Man et al., 2023) and in peats (Yang et al., 2019). Thaumarchaeotal culture studies have reported the presence of OH-isoGDGTs in Group I.1a Thaumarchaeota and SAGMCG-1 (Elling et al., 2014, 2017; Bale et al., 2019) but were not detected in soil Group I.1b Thaumarchaeota (Sinninghe Damsté et al., 2012; Elling et al., 2017). However, they have also been detected in cultures of thermophilic Euryarchaeota (Liu et al., 2012a, b), indicating that OH-isoGDGTs are not exclusive to Thaumarchaeota. In the open ocean,

Table 1
Definitions of isoGDGT and hydroxylated isoGDGT-based proxy indices and their regression correlations with sea water temperatures.

Proxy indices	Equation No.	Equation/regression	n	R ²	Reference
%OH =	1	%OH = -0.24 × SST + 8.3	38	0.59	Huguet et al. (2013)
$\frac{[\text{OH} - 0] + [\text{OH} - 1] + [\text{OH} - 2]}{[0] + [1] + [2] + [3] + [\text{Cren}] + [\text{Cren}'] + [\text{OH} - 0] + [\text{OH} - 1] + [\text{OH} - 2]} \times 100$	2	%OH = -0.227 × SST + 6.79	469	0.73	This study (NIOZ dataset)
	3	%OH = 0.005 × SST ² - 0.38 × SST + 7.64	469	0.75	This study (NIOZ dataset)
	4	%OH = -0.306 × SST + 8.87	667	0.65	This study (complete dataset)
RI - OH = $\frac{[\text{OH} - 1] + 2 \times [\text{OH} - 2]}{[\text{OH} - 1] + [\text{OH} - 2]}$	5	RI - OH = 0.018 × SST + 1.11	107	0.74	Lü et al. (2015)
	6	RI - OH = 0.021 × SST + 1.06	469	0.79	This study (NIOZ dataset)
	7	RI - OH = 0.0006 × SST ² + 0.002 × SST + 1.17	469	0.83	This study (NIOZ dataset)
RI - OH' = $\frac{[\text{OH} - 1] + 2 \times [\text{OH} - 2]}{[\text{OH} - 0] + [\text{OH} - 1] + [\text{OH} - 2]}$	8	RI - OH = 0.018 × SST + 1.12	744	0.79	This study (complete dataset)
	9	RI - OH' = 0.0422 × SST - 0.029	167	0.76	Fietz et al. (2020)
	10	RI - OH' = 0.044 × SST - 0.11	469	0.64	This study (NIOZ dataset)
	11	RI - OH' = 0.0007 × SST ² + 0.02 × SST + 0.03	469	0.66	This study (NIOZ dataset)
OH ^C = $\frac{[2] + [3] + [\text{Cren}'] - [\text{OH} - 0]}{[1] + [2] + [3] + [\text{Cren}'] + [\text{OH} - 0] + [\text{OH} - 1] + [\text{OH} - 2]}$	12	RI - OH' = 0.040 × SST + 0.003	759	0.71	This study (complete dataset)
	13	OH ^C = 0.0266 × SST - 0.144	52	0.88	Fietz et al. (2016)
	14	OH ^C = 0.046 × SST - 0.59	469	0.86	This study (NIOZ dataset)
	15	OH ^C = -0.0008 × SST ² + 0.07 × SST - 0.73	469	0.88	This study (NIOZ dataset)
	16	OH ^C = 0.043 × SST - 0.53	555	0.85	This study (complete dataset)
TEX ₈₆ ^{OH} = $\frac{[2] + [3] + [\text{Cren}']}{[1] + [2] + [3] + [\text{Cren}'] + [\text{OH} - 0]}$	17	TEX ₈₆ ^{OH} = 0.023 × SST + 0.033	513	0.88	This study (NIOZ dataset)
	18	TEX ₈₆ ^{OH} = 0.021 × SST + 0.08	599	0.88	This study (complete dataset)
	19	TEX ₈₆ ^{OH} = 0.026 × Temperature _{0-200m} + 0.09	470	0.89	This study (NIOZ dataset)
TEX ₈₆ = $\frac{[2] + [3] + [\text{Cren}']}{[1] + [2] + [3] + [\text{Cren}']}$	20	TEX ₈₆ ^{OH} = 0.025 × Temperature _{0-200m} + 0.11	556	0.90	This study (complete dataset)
	21	TEX ₈₆ = 0.014 × SST + 0.28	513	0.78	This study (NIOZ dataset)
	22	TEX ₈₆ = 0.012 × SST + 0.33	662	0.78	This study (complete dataset)

[OH - n] indicates hydroxylated isoprenoidal GDGTs with n number of cyclopentane rings.

[n] indicates non-hydroxylated isoprenoidal GDGTs with n number of cyclopentane rings.

Thaumarchaeota are considered the dominant source of isoGDGTs (Zeng et al., 2019; Besseling et al., 2020) and this likely holds for OH-isoGDGTs. A common source of OH-isoGDGTs and non-hydroxylated isoGDGTs in these environments is supported by the strong correlations observed between the concentration of OH-isoGDGTs and crenarchaeol (specific to Thaumarchaeota; Sinninghe Damsté et al., 2002; Bale et al., 2019) as well as 16S rRNA gene abundances of Group I.1a Thaumarchaeota in suspended particulate matter in both the marine (Sollai et al., 2019) and lacustrine (Sinninghe Damsté et al., 2022b) water column.

OH-isoGDGTs have been shown to be more abundant at higher latitudes in the global ocean, and their abundance relative to isoGDGTs (%OH; Table 1) showed a significant negative correlation with sea surface temperature (SST) (Huguet et al., 2013). A molecular dynamics simulation study with hydroxylated and non-hydroxylated isoGDGT-0 has shown that the hydroxy group of OH-isoGDGTs extends the polar head group region by bulging out of the inner core lipid and forming hydrogen bonds with water molecules and sugar moieties of adjacent lipids (Huguet et al., 2017). An increase in the relative abundance of OH-isoGDGTs may, thus, serve as an adaptation to low temperatures for the archaeal cell, as the hydroxy group creates free cavities in the inner core lipids and increases the overall fluidity of the membrane (Huguet et al., 2017).

Several indices have been developed to quantify the presumed temperature control on OH-isoGDGT distributions and abundance, such as the ring index of OH-isoGDGTs, RI–OH and RI–OH' (Table 1), based on changes in the number of cyclopentane moieties (Lü et al., 2015). For the currently available global dataset ($n < 170$), the RI–OH and RI–OH' proxies show positive correlations with SST ($R^2 > 0.70$), though with considerable scatter (Lü et al., 2015; Fietz et al., 2020). Early applications of these proxies specifically targeted high-latitude sediments (Fietz et al., 2013, 2016; Kremer et al., 2018; Vorrath et al., 2020; Wu et al., 2020; Allaart et al., 2020), although recent studies have also shown their potential as a temperature proxy in temperate and tropical regions (Davtian et al., 2019, 2021; Morcillo-Montalbá et al., 2021; Liu et al., 2022; Varma et al., 2023; Davtian and Bard, 2023). These OH-isoGDGT-based proxies often infer temperature trends/variability similar to other proxies studied (U_{37}^K , TEX_{86}^L , TEX_{86}^H , Long chain Diol Index) and have been applied successfully in multi-proxy studies of the past climate.

Although promising, several studies indicate potential issues with the application of OH-isoGDGT-based proxies. Surface sediment studies from the Southern Ocean suggested that the RI–OH' reflects sub-surface temperatures rather than SST in the Antarctic region (Liu et al., 2020; Lamping et al., 2021). Furthermore, several studies have suggested a possible seasonal bias of RI–OH or RI–OH' proxies to winter/spring in the Mediterranean and the Beaufort Sea (Davtian et al., 2019; Wu et al., 2020) or to the summer monsoon season in the South China Sea (Wei et al., 2020) as well as depth biases during glacial periods (Fietz et al., 2016; Davtian et al., 2019; Morcillo-Montalbá et al., 2021; Liu et al., 2022). A larger change in RI–OH and RI–OH' temperatures compared to those inferred by U_{37}^K and/or TEX_{86} has been observed during climate events like Heinrich Stadials, Dansgaard-Oeschger cycles or glacial-interglacial cycles at different locations (Davtian et al., 2019, 2021; Morcillo-Montalbá et al., 2021; Varma et al., 2023). A warm bias of the RI–OH proxy was observed for coastal sediments receiving high amounts of terrestrial input (Kang et al., 2017). Xiao et al. (2023) suggested an influence of water depth on OH-isoGDGT resulting in a potential underestimation of reconstructed SST when RI–OH' is used in deep sea sediments. A difference in the OH-isoGDGT distributions between deep and shallow water archaeal communities has also been suggested (Zhu et al., 2016; Lü et al., 2019). Furthermore, a recent Baltic Sea study suggested that salinity may also have an impact on the distribution of OH-isoGDGTs (Sinninghe Damsté et al., 2022a). Thus, although previous studies on OH-isoGDGT-based proxies have shown

their potential as a seawater temperature proxy, they also highlighted the need for better constraints of the controls on OH-isoGDGT distributions (e.g. Davtian et al., 2021; Varma et al., 2023). Studies on cultures of archaea have revealed large variations in the composition of OH-isoGDGTs among different strains but a correlation between the abundance of OH-isoGDGTs relative to all the isoGDGTs and growth temperature was not observed (Elling et al., 2014, 2017; Bale et al., 2019). An enrichment culture of Thaumarchaeota from the Baltic Sea, grown at both 4 and 22 °C, also exhibits no significant change in %OH with temperature (Sinninghe Damsté et al., 2022a). However, the culture exhibits a dominance of OH-isoGDGT-0 at lower temperature and OH-isoGDGT-2 at higher temperature, which is consistent with the results found in environmental samples. In contrast to U_{37}^K and TEX_{86} , OH-isoGDGT-based proxies lack extensive investigations on the distribution of OH-isoGDGTs in globally distributed surface sediments from widely different geographical regions.

Here we substantially extend the existing dataset of the distribution of OH-isoGDGTs in marine surface sediments and evaluate the impact of different environmental parameters on OH-isoGDGT distributions, together with those of non-hydroxylated isoGDGTs, and the applicability of proxies based on OH-isoGDGTs. Our findings provide new constraints on OH-isoGDGT-based paleothermometers, allowing us to develop a new proxy index for paleotemperature reconstruction.

2. Materials and methods

2.1. Surface sediments and compilation

For this study, we re-analyzed or re-integrated the mass chromatograms of 575 surface sediments previously analyzed at NIOZ. These include surface sediments from a global TEX_{86} calibration study (Kim et al., 2010), a global long-chain diol calibration study (de Bar et al., 2020) and surface sediments from the Baltic Sea (Sinninghe Damsté et al., 2022a). For an overview, see Supplementary Table S1 and Fig. 1. In all these studies, OH-isoGDGTs were quantified by integrating the peaks that correspond to $[M + H-18]^+$ ions (i.e., m/z 1300, 1298 and 1296).

2.2. Sediment core

To explore the potential of OH-isoGDGT-based proxies for paleotemperature reconstruction, we analyzed the sediment core Co1010, retrieved from Prydz Bay in the Southern Ocean (68.80°S, 77.89°E) from a water depth of ~38 m (for more details, see Wagner et al., 2008; Berg et al., 2010). The modern annual mean SST at this location is -0.3 °C (Locarnini et al., 2019). The age model for the sediment core is based on Berg et al. (2020) and the ^{14}C calibration curve was updated according to Heaton et al. (2020). We analyzed a total of 64 sediment horizons which spans the last ~11,000 years, with an average sampling resolution of one sample per ~170 years. We also explored the published paleorecords from ODP Site 1235 and 1078 (Varma et al., 2023) for newly developed OH-isoGDGT-based proxies.

2.3. GDGT analysis

The lipid extraction methods used for the surface sediments analyzed at NIOZ are described in the original literature and to a large degree summarized by de Bar et al. (2020) (see Supplementary Table S1 for an overview). Since these previous analyses (Kim et al., 2010; de Bar et al., 2020) were performed using a method with a shorter run time, whereby the OH-isoGDGTs did not elute from the column, re-analysis was needed. For re-analysis, the original polar fractions of the extracts of the surface sediments obtained by Kim et al. (2010) and de Bar et al. (2020) were dissolved in hexane:isopropanol (99:1, v:v), filtered through a 0.45 µm PTFE filter, and analyzed with ultra-high performance liquid

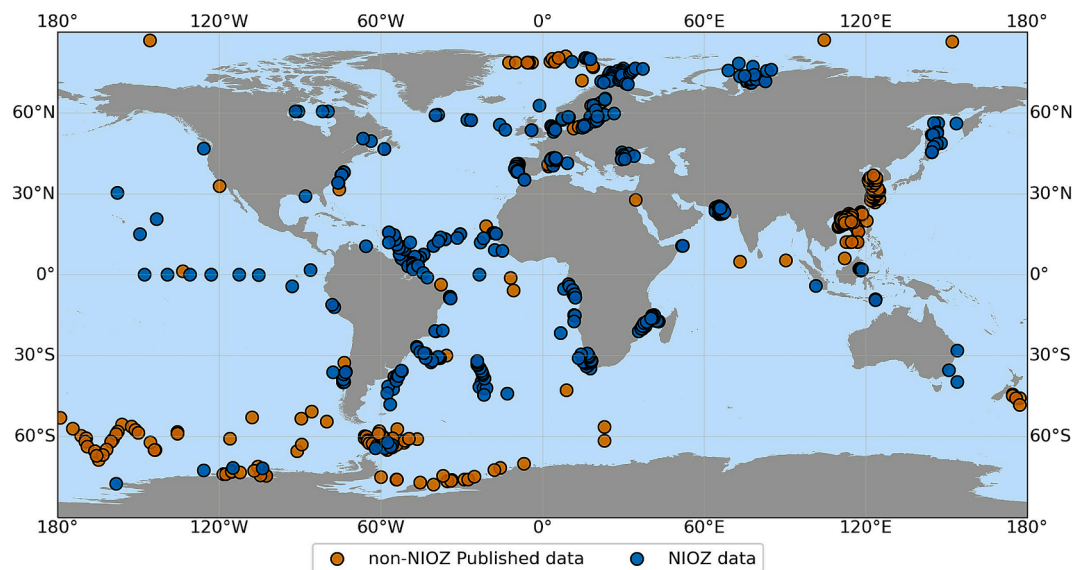


Fig. 1. Location of the surface sediments ($n = 872$) for which the distribution of OH-isoGDGTs has been studied. The surface sediments investigated in this study at NIOZ (including the published data from [Sinninghe Damsté et al., \(2022a\)](#)) are represented by blue dots ($n = 575$). The surface sediments studied by [Fietz et al., \(2016, 2020\)](#), [Yang et al. \(2018\)](#), [Wei et al. \(2020\)](#) and [Lamping et al. \(2021\)](#) are indicated by orange dots ($n = 297$). (For interpretation of the references to colour in this figure legend, the reader is referred to the web version of this article.)

chromatography/ mass spectrometry (UHPLC/MS) on an Agilent 1260 Infinity HPLC coupled to an Agilent 6130 MSD according to [Hopmans et al. \(2016\)](#). The isoprenoid and branched GDGTs were detected in Selective Ion Monitoring (SIM) mode for protonated GDGT molecules $[M + H]^+$ and OH-isoGDGTs were quantified by integration of the appropriate peaks in the mass chromatograms of the $[M + H-18]^+$ ions (i.e., m/z 1300, 1298 and 1296) as has been done previously ([Huguet et al., 2013](#)). The OH-isoGDGTs were identified by comparing retention times to an in-house standard from a Drammensfjord sediment extract. Additionally, two sediments from the tropical Atlantic and the Baltic Sea were analyzed for $[M + H]^+$ ions of m/z 1318, 1316 and 1314 to examine the relative amount of $[M + H-18]^+$ versus $[M + H]^+$ ions of OH-isoGDGTs. Strict quality control was performed on all GDGTs by ensuring that the peak integration area is above the limit of quantification for the instrument and that each peak's signal-to-noise ratio was higher than 10.

For sediment core Co1010, the sediments were freeze-dried and extracted using a modified Bligh & Dyer extraction method (BDE) ([Bligh and Dyer, 1959](#); [Sturt et al., 2004](#); [Bale et al., 2021](#)). The sediments were extracted thrice ultrasonically in a mixture of methanol (MeOH), dichloromethane (DCM), and phosphate buffer (2:1:0.8, v:v:v) for 10 min. The supernatant was collected after the mixture was centrifuged for 2 min at 3000 rpm. The combined supernatants were phase separated by adding additional DCM and phosphate buffer to achieve a final solvent ratio of 1:1:0.9 (v:v:v). The organic phase was collected after centrifuging the mixture for 2 min at 3000 rpm, and the aqueous phase was then extracted thrice using DCM. These steps were repeated on the same sediment but with a mixture of MeOH, DCM, and trichloroacetic acid (2:1:0.8, v:v:v). The extracts were dried under N_2 gas until ~ 1 ml of solvent remained and desulphurized with copper turnings, activated with 2 N HCl overnight, and eluted over a Na_2SO_4 column using DCM:MeOH (9:1, v:v). The extracts were dried under a stream of N_2 and separated into apolar, ketone and polar fractions using an activated Al_2O_3 column with hexane:DCM (9:1, v:v), hexane:DCM (1:1, v:v) and DCM:MeOH (1:1, v:v) mixtures, respectively. The polar fractions containing isoGDGTs were dissolved in hexane:isopropanol (99:1, v:v), filtered through a 0.45 μm PTFE filter, and analyzed on the UHPLC/MS as mentioned above.

2.4. Environmental data

The environmental data from the surface sediment locations were obtained from the World Ocean Atlas 2018 (WOA18) database. The annual mean sea surface temperature (0 m), sub-surface temperature (0–200 m, calculated as described in [Kim et al., 2008](#)), salinity and nitrate data were obtained for each location from the corresponding $1^\circ \times 1^\circ$ grid box ([Garcia et al., 2018](#); [Locarnini et al., 2019](#); [Zweng et al., 2019](#)). For some surface sediments relatively close to the coast lacking 1° grid temperature data resolution, we extended the grid size to 2° , especially for surface sediments from high latitudes near the Arctic and Antarctica or from the delta regions. The surface sediments from the Rhône delta in the Gulf of Lions were sampled at high resolution close to the coast, and therefore NSIPP AVHRR (Advanced Very High Resolution Radiometer) SST data were previously used by [Kim et al. \(2015\)](#). In this study, we also employ the AVHRR SST data from [Kim et al. \(2015\)](#) for the surface sediments from the Rhône delta, instead of coarser WOA18 data.

2.5. Statistical analysis

Principal Component Analysis (PCA) was performed on the summed and standardized fractional abundances of both OH- and non-hydroxylated isoGDGTs, annual mean SST, salinity, nitrate, and water depth data using the `prcomp` function in R software. Regression analysis between various parameters done in this study was performed using statistical functions in python (`scipy.stats`).

To examine the variations in the analysis of OH-isoGDGTs among different laboratories, we conducted statistical tests to determine if there are any differences in the mean proxy values from these laboratories. To do this, we selected a subset of surface sediments from the same geographic region within a 2° grid, but from different laboratories ([Table 2](#)). We performed a one-way analysis of variance (ANOVA) using the `f_oneway` package from `scipy.stats` in python, after ensuring that the assumptions of equal variance and normal distribution were met for each group. If any groups had unequal variance or a non-normal distribution, we instead performed a non-parametric test, Kruskal-Wallis test (using `scipy.stats`) to examine statistical difference between the medians of the groups.

Table 2

Results of one-way ANOVA tests (or Kruskal-Wallis test, denoted by asterisk *) at significance level of 0.05 for (a) RI –OH', (b) %OH and (c) $\text{TEX}_{86}^{\text{OH}}$ obtained from surface sediments from the same geographical regions (within a $2^\circ \times 2^\circ$ grid) but reported by different labs. Values in bold indicate statistically significant values ($p < 0.05$).

Proxy	Labs	Region	F value	p value
(a)RI –OH'	NIOZ (n = 6), AWI (n = 5)	Antarctic	0.0*	1*
	NIOZ (n = 13), Leibniz IOW (n = 33)	Baltic Sea	4.92	0.032
	BGEG Wuhan (n = 11), AWI (n = 11)	South China Sea	0.88	0.359
(b)%OH	NIOZ (n = 6), AWI (n = 5)	Antarctic	74.21	< 0.0001
	NIOZ (n = 13), Leibniz IOW (n = 33)	Baltic Sea	149.13	< 0.0001
	NIOZ (n = 6), AWI (n = 5)	Antarctic	7.5*	0.006*

3. Results

For this study, we used a set of surface sediments that have previously been analyzed for biomarker proxies at NIOZ, comprising 221 surface sediments that were previously utilized for a global TEX_{86} calibration study (Kim et al., 2010) and 341 surface sediments utilized for a global long-chain diol calibration study (de Bar et al., 2020). This collection has a wide geographical distribution (Fig. 1) including sediments from the Mozambique Channel (Schulz et al., 2011; Fallet et al., 2012), the coast of Australia (Smith et al., 2013), the North Sea (Bale et al., 2013), the Amazon shelf (Zell et al., 2014), the Kara Sea (De Jonge et al., 2015), the Iberian margin (Kim et al., 2016), the Berau delta (Sinninghe Damsté, 2016), the Okhotsk Sea (Lo et al., 2018), the Black Sea (Lattaud et al., 2018) and the tropical Atlantic (Bale et al., 2018). The polar fractions of these sediments were re-analyzed for isoGDGTs and OH-isoGDGTs following the methodology of Hopmans et al. (2016). In addition, OH-isoGDGT data from thirteen surface sediments from the Baltic Sea previously analyzed at NIOZ following the same methods (Sinninghe Damsté et al., 2022a) were added as well. To ensure consistency in data handling between sample sets, the mass chromatograms used to quantify isoGDGTs and OH-isoGDGTs of these Baltic Sea sediments were re-integrated.

We first screened the newly acquired dataset of surface sediments (see Supplementary Table S1 for data) ($n = 575$) for potential terrestrial input, as it may cause biases in OH-isoGDGT-based proxy values (Kang et al., 2017; Wei et al., 2020; Man et al., 2023). In marine sediments, the Branched and Isoprenoid Tetraether index (BIT) (Hopmans et al., 2004; De Jonge et al., 2015) has often been used as an indicator of a potential contribution of terrestrial GDGTs, with a cutoff value of 0.3 used as a threshold for application of the TEX_{86} index (e.g. Weijers et al., 2006). We do note that this threshold is fairly arbitrary since the threshold for potential bias will likely vary with geographical region and because the brGDGTs can also be produced *in-situ* in the marine environment (e.g. Peterse et al., 2009; Zell et al., 2014b; Sinninghe Damsté, 2016; Xiao et al., 2016). Nevertheless, this threshold has generally been applied in previous paleoclimate studies and appears to have been effective (Schouten et al., 2013b). We identified 52 surface sediments from the Rhône delta, the Berau delta, the Eastern South Atlantic, the Mozambique Channel, the Pakistan Margin, the South China Sea, the Amazon shelf, the Baltic Sea, the Siberian coast and the Kara Sea from our dataset with BIT values > 0.3 . Although further studies are required to examine the influence of terrigenous source on OH-isoGDGT-based proxies, we excluded these 52 surface sediments from further analysis to avoid potential biases. One surface sediment from the North Atlantic was considered as an outlier and was removed from the dataset due to unusually high TEX_{86} and RI –OH' values compared to other sediments from the same region. Although Thaumarchaeota are the main producers of OH-isoGDGTs and isoGDGTs in the marine environment (see

Introduction), we also screened our dataset for the potential influence of archaea involved in methane cycling through isoGDGT [2]/cren-archaeol ratio and Methane Index (Weijers et al., 2011; Zhang et al., 2011), which resulted in low values (< 0.3 and < 0.5 , respectively), confirming no major influence of archaea involved in anaerobic methane oxidation. We found 53 surface sediments, mostly from tropical regions where OH-isoGDGT-1 and –2 were below the detection limit, which were excluded from further analysis.

The percentage of hydroxylated isoGDGTs (%OH) in the remaining dataset ($n = 469$; referred to in the following text as the 'NIOZ dataset') ranges from only 0.06 % in the warm Arabian Sea to 10.6 % in the cold Okhotsk Sea (Fig. 2). As observed previously (Huguet et al., 2013), the abundance of OH-isoGDGTs increases with latitude, i.e., the average % OH is 0.97 ± 0.5 % in the subtropical-tropical region (30°N – 30°S), 3.2 ± 1.8 % in the temperate region (30°N – 60°N and 30°S – 60°S), and 6.6 ± 1.9 % in the subpolar-polar region (60°N – 90°N and 60°S – 90°S) (Fig. 2). Besides the change in the abundance of OH-isoGDGTs relative to regular isoGDGTs, we also observe a latitudinal change within the internal distribution of OH-isoGDGTs in the NIOZ dataset (Figure S1). In general, OH-isoGDGT-0 shows the highest relative abundance in polar regions and decreases in abundance towards the tropics, while the relative abundances of OH-isoGDGT-1 and –2 decrease with latitude.

4. Discussion

4.1. Consistency between laboratories in analyzing OH-isoGDGTs

We first compared our dataset with OH-isoGDGT data obtained in other laboratories ($n = 297$; 'non-NIOZ' dataset; see Fig. 1 for geographical locations). The non-NIOZ dataset includes a total of 164 surface sediments from various studies comprising a global dataset from Huguet et al. (2013), surface sediments from the Arctic region (Fietz et al., 2013), the Chinese coastal seas (Lü et al., 2015), and the Baltic and the North Sea (Kaiser and Arz, 2016) as summarized in Fietz et al. (2020). Additional OH-isoGDGT data from a total of 133 surface sediments from the South China Sea (Yang et al., 2018; Wei et al., 2020), the South Pacific region (Fietz et al., 2016) and the Southern Ocean (Lamping et al., 2021) have also been included here. Some studies did not provide peak areas of both isoGDGTs and OH-isoGDGTs, and, therefore, proxy indices that use both isoGDGTs and OH-isoGDGTs could not always be calculated. A similar check on terrestrial influence was performed for the non-NIOZ dataset, using the BIT index wherever BIT values were reported. Previous studies have reported BIT values < 0.3 , so we concluded that there was no terrestrial influence on the distributions of isoGDGTs and OH-isoGDGTs in any of the surface sediments from the non-NIOZ dataset.

An important consideration when comparing the NIOZ and the non-

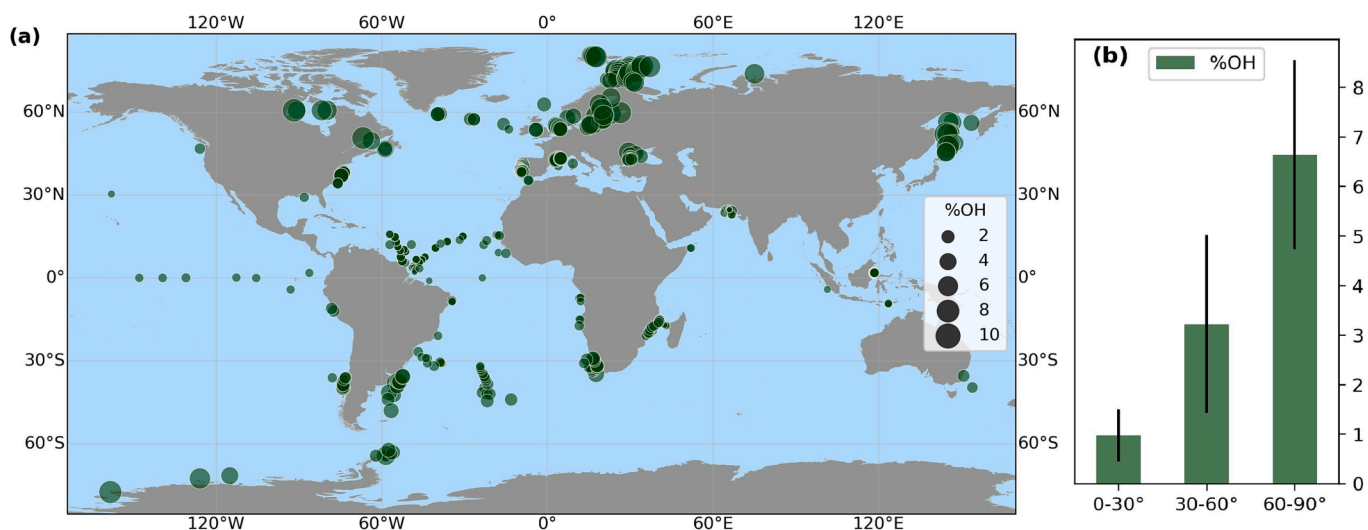


Fig. 2. The abundance of OH-isoGDGTs relative to that of isoGDGTs in global ocean surface sediments from the NIOZ dataset. (a) Global distribution of values for %OH, indicated by bubble size. (b) Bar plot indicating the average %OH values in (sub)tropical (0-30°), temperate (30-60°) and (sub)polar (60-90°) regions. The error bars indicate the standard deviation of the mean.

NIOZ datasets is that the analytical equipment in various laboratories may differ and, perhaps, yield different quantitative results for OH-isoGDGT-based proxies from the same surface sediments. Generally, such issues can be assessed by round-robin studies (e.g. Rosell-Melé et al., 2001; Schouten et al., 2009, 2013a), but such a study has not been performed yet for OH-isoGDGTs. Interlaboratory studies performed for GDGTs show similar results for quantification of isoGDGTs (i.e., TEX_{86}) but large differences in the quantification of isoGDGTs versus brGDGTs (i.e., determination of the BIT index) occur between laboratories. This has been attributed to the difference in response between mass spectrometers in various laboratories (Schouten et al., 2009, 2013a). These results suggest that quantification may be comparable across laboratories within the same GDGT compound class but different between compound classes (i.e., non-hydroxylated isoGDGTs and OH-isoGDGTs). Indeed, when comparing the cross-plots of the complete global dataset for a proxy that relates OH-isoGDGTs to regular isoGDGTs (%OH; Fig. 3b), with a proxy index that only utilizes OH-isoGDGTs (RI-OH; Fig. 3a), we notice that data point clusters from other laboratories tend to deviate to a larger extent from those of the NIOZ dataset for %OH than with RI-OH.

To investigate whether proxy values depend on the lab where they

have been determined, we selected surface sediments from both the NIOZ and the non-NIOZ datasets from the same geographic region (within a 2° grid) in cases where multiple laboratories have reported results, assuming there are no major sedimentological or environmental differences between the different samples of the different labs. Comparison of proxy values reported for the Antarctic, the Baltic Sea and the South China Sea surface sediments shows that for the Antarctic region and the South China Sea, we cannot reject the null hypothesis that there is no difference among the median or mean RI-OH values, respectively, from different laboratories ($p > 0.3$) at the significance level of 0.05 (Table 2). However, for the Baltic Sea, mean RI-OH values differ significantly between laboratories ($p = 0.032$). For the %OH, significant differences between mean proxy values from different laboratories were observed for both the Baltic Sea and the Antarctic region ($p < 0.0001$) at the significance level of 0.05 (Table 2). This suggests potential differences in the quantification of OH-isoGDGTs versus regular isoGDGTs between laboratories, as previously suggested by Sinnighe Damsté et al., (2022a) for the Baltic Sea sediments.

There are two potential analytical explanations for these differences: (i) different ionization efficiencies of OH-isoGDGTs versus regular isoGDGTs between instruments or (ii) different degrees of in-source

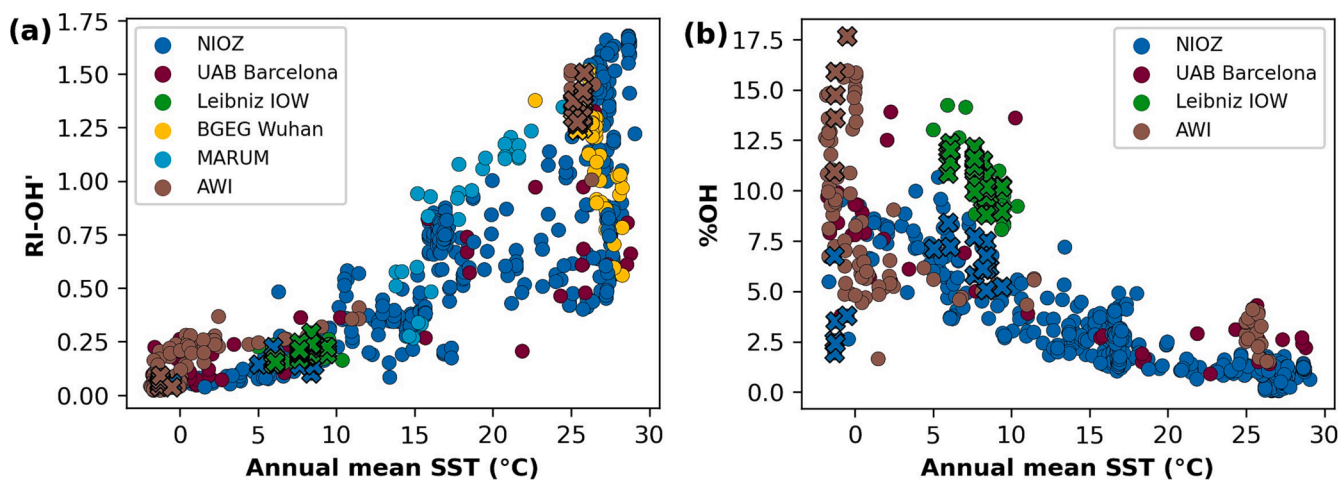


Fig. 3. Cross-plot of (a) RI-OH' and (b) %OH against annual mean SST for the complete global dataset analyzed in different laboratories. Surface sediments used for statistical tests to check for interlaboratory differences are represented by crosses (see Table 2).

dehydration leading to different abundances of the $[M + H-18]^+$ versus $[M + H]^+$ ions between the various mass spectrometers used in the different laboratories. To explore the latter, we analyzed the amount of dehydrated product ions ($[M + H-18]^+$) vs. precursor molecular ions ($[M + H]^+$) of OH-isoGDGTs for our instrumental set-up for two surface sediments from the tropical Atlantic and the Baltic Sea. We found that the degree of in-source dehydration is $\sim 90\%$ for OH-isoGDGTs. Comparing the proxy indices calculated from $[M + H-18]^+$ fragments with those calculated on the basis of the $[M + H^{18}]^+$ and $[M + H]^+$ fragments combined, shows a difference of 0.01 RI –OH units for both regions. For %OH we observe a difference of 0.08 % for the tropical Atlantic sediment and 0.59 % for the Baltic Sea sediment. Since the %OH measured at NIOZ tends to be lower than that of other laboratories in these locations (Fig. 3b), it would suggest that full in-source dehydration of OH-isoGDGTs takes place in mass spectrometers operated in other laboratories. However, this difference does not seem to fully explain the difference in %OH in sample clusters from the same geographical location but determined in different laboratories (Fig. 3) and thus differences in ionization efficiencies in the APCI source may also play a role.

Being alerted to potential changes in quantifying OH-isoGDGTs due to potential variation in in-source dehydration, we also examined the changes in values of RI –OH and %OH through time for a period of four years (2019–2022) in our laboratory using an in-house standard from a Drammensfjord sediment extract. We observe that both proxy values remain fairly constant (Fig. S2a, S2b), especially for RI –OH (mean and standard deviation of 0.195 ± 0.007). Therefore, we conclude that the data obtained over this time period in our lab is consistent. Our recommendation for laboratories seeking to apply OH-isoGDGT-based proxies is to use an in-house standard that contains adequate amounts of OH-isoGDGTs as a quality control to ensure consistent OH-isoGDGT signal responses within their laboratory. Furthermore, a round-robin study on OH-isoGDGTs is required to establish whether there are true interlaboratory differences in analyzing OH-isoGDGTs versus isoGDGTs. Due to these potential interlaboratory differences, we use only the results obtained for the NIOZ dataset in the following discussions but will conclude with discussing the consequences for the complete dataset, i.e., the combined NIOZ and non-NIOZ datasets.

4.2. Influence of environmental parameters on OH-isoGDGT distributions

To investigate the environmental controls on the relative abundances

of hydroxylated isoGDGTs, we performed a principal component analysis (PCA) on the normalized fractional abundances of OH-isoGDGTs and non-hydroxylated isoGDGTs (Fig. 4). The first two principal components (PCs) account for 62.6 and 17.4 % of the variance, respectively. IsoGDGT-0, OH-isoGDGT-0 and OH-isoGDGT-1 plot negatively on PC1 and the remaining isoGDGTs and OH-isoGDGT-2 score positively. SST has a strong positive loading along PC1, suggesting that PC1 is likely capturing distributional changes caused by sea temperature. This confirms a major impact of temperature on the distribution of OH-isoGDGTs, especially for OH-isoGDGT-0, as observed previously (Fietz et al., 2013; Huguet et al., 2013). PC2 shows mainly a positive correlation with OH-isoGDGT-1 and –2 as well as isoGDGT-3 and crenarchaeol (Fig. 4). Interestingly, the environmental parameter correlating negatively with PC2 is water depth. This suggests that besides temperature, water depth or environmental parameters strongly associated with water depth might be affecting the distribution of OH-isoGDGT-1 and –2, in agreement with recent observations of Xiao et al. (2023). Other parameters such as surface salinity and nitrate do not seem to have a major impact on the distribution of OH-isoGDGTs and non-hydroxylated isoGDGTs. When the biplot of this dataset (Fig. 4) is compared with the PCA previously performed on non-hydroxylated isoGDGTs in a global set of marine surface sediments (Kim et al., 2010), a similar clustering of variables is revealed, except for isoGDGT-1, which shows a stronger positive correlation with temperature in our dataset.

To further explore the impact of water depth, we correlated it with the fractional abundance of OH-isoGDGTs and %OH. We observe no strong correlations on the global scale ($R^2 < 0.12$), compared to the strong correlation observed for the water depth vs. the isoGDGT [2]/[3] ratio ($R^2 = 0.74$) (Figure S3), which has been previously reported by Taylor et al. (2013) based on the dataset acquired by Kim et al. (2010). We observe that, although most of the surface sediments with high %OH are from shallow sites with water depth < 1000 m (Figure S3), all these surface sediments are from high latitude regions where %OH has been reported to be relatively high (e.g. Huguet et al., 2013). This is because there is an intrinsic lack of surface sediments from deep water sites in high latitude regions in the NIOZ dataset. Hence, sampling bias may have led to the apparent observation that the abundance of OH-isoGDGT appears to be higher at shallow sites. Interestingly, in the PCA biplot (Fig. 4), many surface sediments that cluster together in the second quadrant near OH-isoGDGT-1 are from the Rhône delta and the Iberian

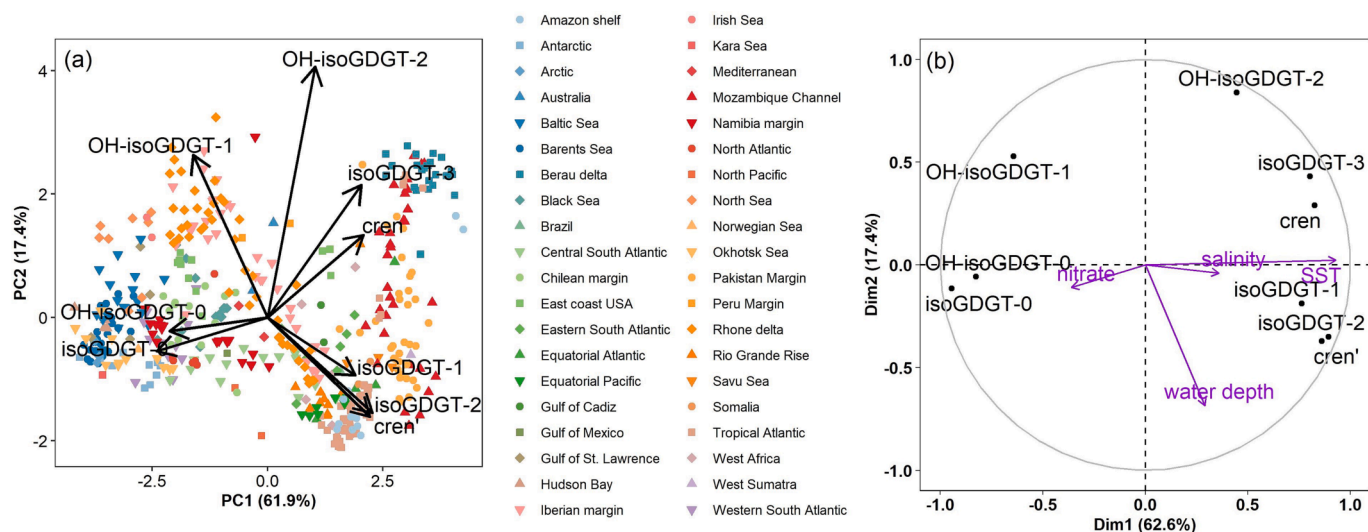


Fig. 4. Principal component analysis of the summed and normalized fractional abundances of both hydroxylated and non-hydroxylated isoGDGTs for the first two components for surface sediments analyzed in the NIOZ laboratory. Panel (a) displays the PCA biplot with surface sediments ($n = 469$) grouped based on geographical regions in the global ocean, and (b) shows loadings for environmental variables for surface sediments for which information was available ($n = 328$), from satellite temperature data or World Ocean Atlas (Locarnini et al., 2019) and loadings of the isoGDGTs.

margin. Water depth is known to strongly influence the isoGDGT distribution in the Mediterranean Sea and Iberian margin (Kim et al., 2015, 2016; Besseling et al., 2019). Indeed, a strong correlation between %OH and water depth ($R^2 = 0.75$) is observed for the Rhône delta and the Iberian margin surface sediments, in contrast to the larger dataset (Figure S3b). It has been reported that deep-water archaeal communities with distinct isoGDGT composition contribute isoGDGTs to the sedimentary pool in restricted basins like the Mediterranean Sea (Kim et al., 2015; Polik et al., 2018). Therefore, potential differences in OH-isoGDGT composition between these archaeal communities might also be evident in the Mediterranean Sea sediments. Hence, OH-isoGDGT distributions, analogous to regular isoGDGTs, might be influenced by water depth (or a related environmental parameter) in the Mediterranean, but less so on a global scale.

4.3. Evaluating the impact of temperature on OH-isoGDGTs and proxies derived from them

4.3.1. Individual OH-isoGDGTs

OH-isoGDGT-based proxies have been used for SST reconstruction (e.g. Davtian et al., 2019; Morcillo-Montalbá et al., 2021; Liu et al., 2022) but the export depths of OH-isoGDGTs remain poorly constrained. Since the likely source organisms of these biomarkers, the Thaumarchaeota, are not restricted to the surface mixed layers (ca. 0–30 m water depth depending on location) (Kamer et al., 2001; Wuchter et al., 2005; Herndl et al., 2005) and that the temperature reconstructed from OH-isoGDGT-based proxies are often interpreted to represent sub-surface temperatures (e.g. Fietz et al., 2016; Davtian et al., 2019, 2021; Morcillo-Montalbá et al., 2021), it is likely that the temperature controlling their distributions is not SST but sub-surface temperature. Nevertheless, it has often been observed that there is a strong correlation between surface and sub-surface temperatures, enabling us to use these paleothermometers for SST reconstructions (cf. Huber, 2010; Schouten et al., 2013b; Tierney, 2013). Therefore, as a first approach, we correlated the relative abundance of OH-isoGDGTs and derived proxies with annual mean SST to explore the impact of temperature, while fully realizing that these are likely not the temperature at which these OH-isoGDGTs, or isoGDGTs, were produced. Cross-correlating the fractional abundances of all isoGDGTs and OH-isoGDGTs with annual mean SST (Figure S4) for the NIOZ dataset, resulted in strongly significant correlations ($p < 0.001$). Strong correlations ($R^2 \geq 0.5$) were observed for all compounds except for OH-isoGDGT-1 and -2, where correlation coefficients were 0.24 and 0.17, respectively (Figure S4). Overall, the cross correlations confirm that temperature is likely the main factor controlling isoGDGT distributions in the global ocean, while other factors are likely impacting

the OH-isoGDGT-1 and -2 distributions, as indicated in our PCA analysis.

When normalizing internally within OH-isoGDGTs and correlating the fractional abundances of OH-isoGDGTs with SST, there is a significant negative correlation between OH-isoGDGT-0 and annual mean SST (linear correlation with $R^2 = 0.72$, $p < 0.001$) and a significant positive correlation for OH-isoGDGT-2 (linear correlation with $R^2 = 0.65$, $p < 0.001$) (Fig. 5). OH-isoGDGT-1 shows a weaker positive correlation with $R^2 = 0.41$, $p < 0.001$. These correlations with SST are consistent with previous studies reporting a strong latitudinal trend in the distribution of OH-isoGDGTs (Fietz et al., 2013; Lü et al., 2015). Note that we used linear correlation as an illustration of the relationship between isoGDGT distributions and SST, but it is evident that some of the correlations are better fitted using other, e.g. quadratic functions. Yang et al. (2018) observed a strong negative correlation of SST with the fractional abundance of OH-isoGDGT-2 normalized to total OH-isoGDGTs for sediments from the South China Sea and suggested its potential as an SST proxy for regions with SSTs greater than 25 °C. However, surface sediments from regions with temperatures > 25 °C only in the NIOZ dataset show no such correlation ($R^2 < 0.10$; data not shown).

4.3.2. OH-isoGDGT-based proxies

There are four proxies using OH-isoGDGTs that have been proposed as proxies for seawater temperature, i.e., %OH, RI-OH, RI-OH' and OH^C (for definitions see Table 1). The relative abundance of OH-isoGDGTs (%OH), as expected from its latitudinal variations, shows a strong negative correlation (linear correlation with $R^2 = 0.73$, $p < 0.001$) with SST in the NIOZ dataset (Fig. 6c). However, surface sediments from the Southern Ocean show a wide range of %OH values, from ~ 2–10 % for a relatively small temperature range (Fig. 6c). Similar large ranges have also been observed for the %OH values in other surface sediments from the Southern Ocean (Lamping et al., 2021). A recent study from Prydz Bay suggested that OH-isoGDGT-based proxies represent sub-surface temperatures (100–200 m) in the Antarctic region and show a decreasing trend in abundance from the shelf to the open ocean (Liu et al., 2020). We observe that most of the Antarctic surface sediments in the NIOZ dataset are from water depths < 2000 m and have isoGDGT [2]/[3] ratio of < 5, indicating a dominant contribution of shallow water thaumarchaeotal ecotypes to the sedimentary isoGDGTs (Taylor et al., 2013). The corresponding %OH of the Antarctic surface sediments ranges from 1.9 to 9.5 % in the NIOZ dataset, suggesting large variations in OH-isoGDGT of shallow water thaumarchaeotal communities, despite similar annual mean temperatures. Potentially, this could be caused by strong seasonal variations in OH-isoGDGT production in polar regions.

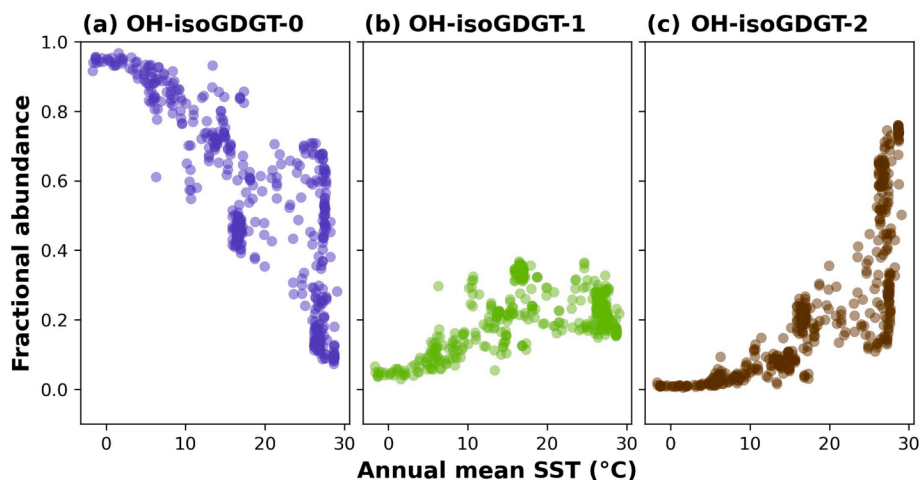


Fig. 5. Fractional abundance of individual OH-isoGDGTs to total OH-isoGDGT pool ($n = 469$) in surface sediments analyzed in the NIOZ laboratory versus annual mean SST for (a) OH-isoGDGT-0, (b) OH-isoGDGT-1, and (c) OH-isoGDGT-2.

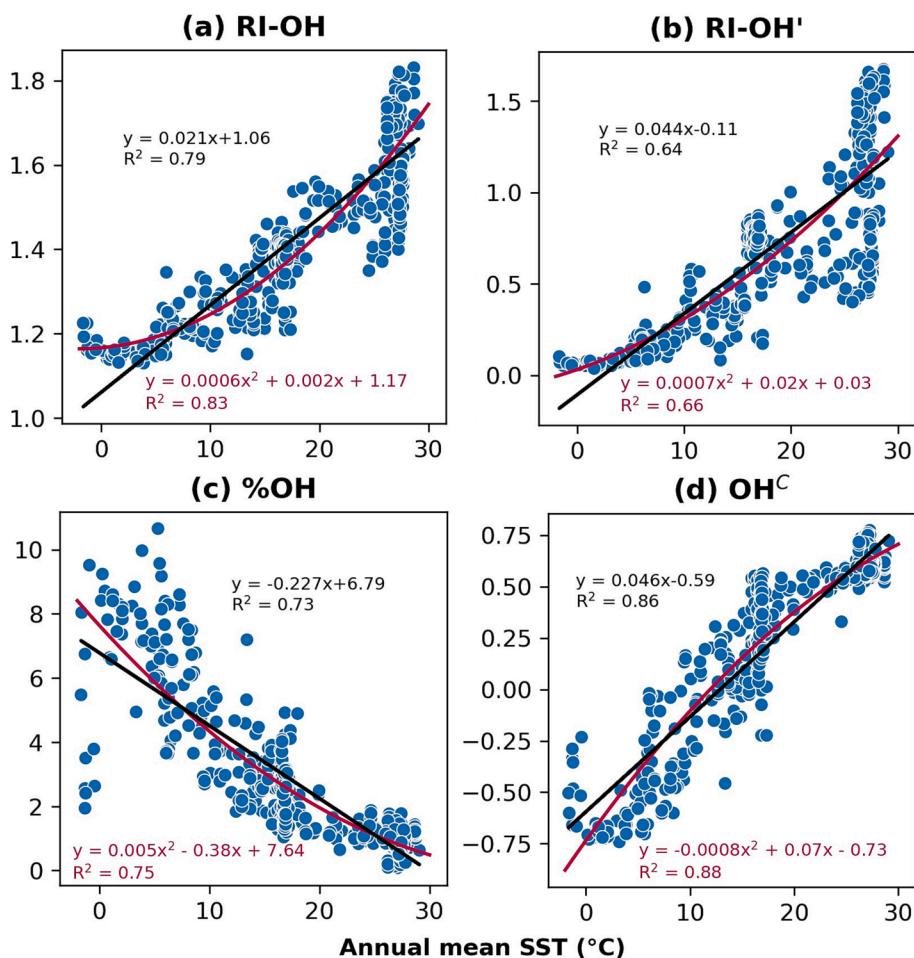


Fig. 6. Correlations of previously proposed OH-isoGDGT-based proxies with annual mean SST for surface sediments analyzed in the NIOZ laboratory ($n = 469$): (a) RI-OH, (b) RI-OH', (c) %OH, and (d) OH^C. Both linear correlations (in black) as well as quadratic correlations (in red) are shown as well as their respective regressions. (For interpretation of the references to colour in this figure legend, the reader is referred to the web version of this article.)

Two other proposed proxies based only on the OH-isoGDGTs are RI-OH and RI-OH' which both express their number of cyclopentane moieties. Lü et al. (2015) suggested the application of RI-OH in warm regions with annual mean SST > 15 °C and RI-OH' in cold < 15 °C regions due to the smaller residuals of the latter in cold regions. We observe a strong correlation of RI-OH with SST (linear correlation with $R^2 = 0.79$, $p < 0.001$) and a weaker correlation of RI-OH' with SST (linear correlation with $R^2 = 0.64$, $p < 0.001$) in the NIOZ dataset (Fig. 6a, 6b). The RI-OH' shows a low sensitivity to changes in SST for temperatures < 5 °C. The correlation coefficient for the RI-OH'-SST correlation is substantially lower than that reported by Fietz et al. (2020) for a smaller dataset ($n = 167$) ($R^2 = 0.76$ versus 0.64 for our dataset), suggesting additional scatter has been introduced. In contrast, the correlation coefficient of RI-OH with SST is slightly higher than in the calibration of Lü et al. (2015) (0.79 versus 0.74, respectively).

Inspection of the correlations of RI-OH and RI-OH' with SST shows that the scatter is especially large at high temperatures (> 25 °C), likely due to low abundance of OH-isoGDGTs in these regions (Fig. 4), which could lead to larger errors in quantification. Furthermore, OH-isoGDGT-2, which is the predominant OH-isoGDGT at high temperatures, may be impacted by other factors such as water depth (see above). Indeed, inspection of the data of the tropical surface sediments with an unusually large range of RI-OH' (and RI-OH) values shows that surface sediments from greater water depths tend to have lower OH-isoGDGT ring index values than sediments from shallower depths (Figure S7a-b, S8a). A correlation of RI-OH' (and RI-OH) with isoGDGT [2]/[3] ratio for

the tropical surface sediments shows a strong non-linear correlation ($R^2 = 0.94$ and 0.85 for RI-OH' and RI-OH, respectively) (Figure S7c, S8b). Thus, the OH-isoGDGT distributions in tropical oceans might be influenced by contributions from greater depths where OH-isoGDGTs are either reflecting the colder deep temperatures or are reflecting deep-water archaeal communities which are known to have distinctly higher isoGDGT [2]/[3] ratios (Villanueva et al., 2015; Zhu et al., 2016; Besseling et al., 2019). Our results are in line with the findings of Xiao et al. (2023), who also showed that the relative abundance of OH-isoGDGTs are influenced by water depth, resulting in lower RI-OH' values. The impact of water depth is not visible in the correlation of % OH with SST (Figure S7d), possibly due to the generally low abundances of OH-isoGDGTs in the tropics. Regardless, care should be taken when using RI-OH' and RI-OH in tropical regions. Xiao et al. (2023) also suggested multi-variable relationships between SST, water depth, and RI-OH', which may vary depending on the latitudinal region. Furthermore, more research is needed to explore the global effects of water depth on OH-isoGDGT based proxies, as our dataset does not contain sufficient surface sediments from deep sites in high-latitude regions.

Fietz et al. (2016) suggested another proxy, the OH^C index, in which both the fractional abundances of OH-isoGDGTs and non-hydroxy isoGDGTs are combined in a modified version of TEX₈₆ (Table 1). Plotting the OH^C index versus annual mean SST for the NIOZ dataset (Fig. 6d) shows a significant correlation ($p < 0.001$, $R^2 = 0.86$), an even stronger correlation than that of TEX₈₆ for the same dataset ($R^2 = 0.78$;

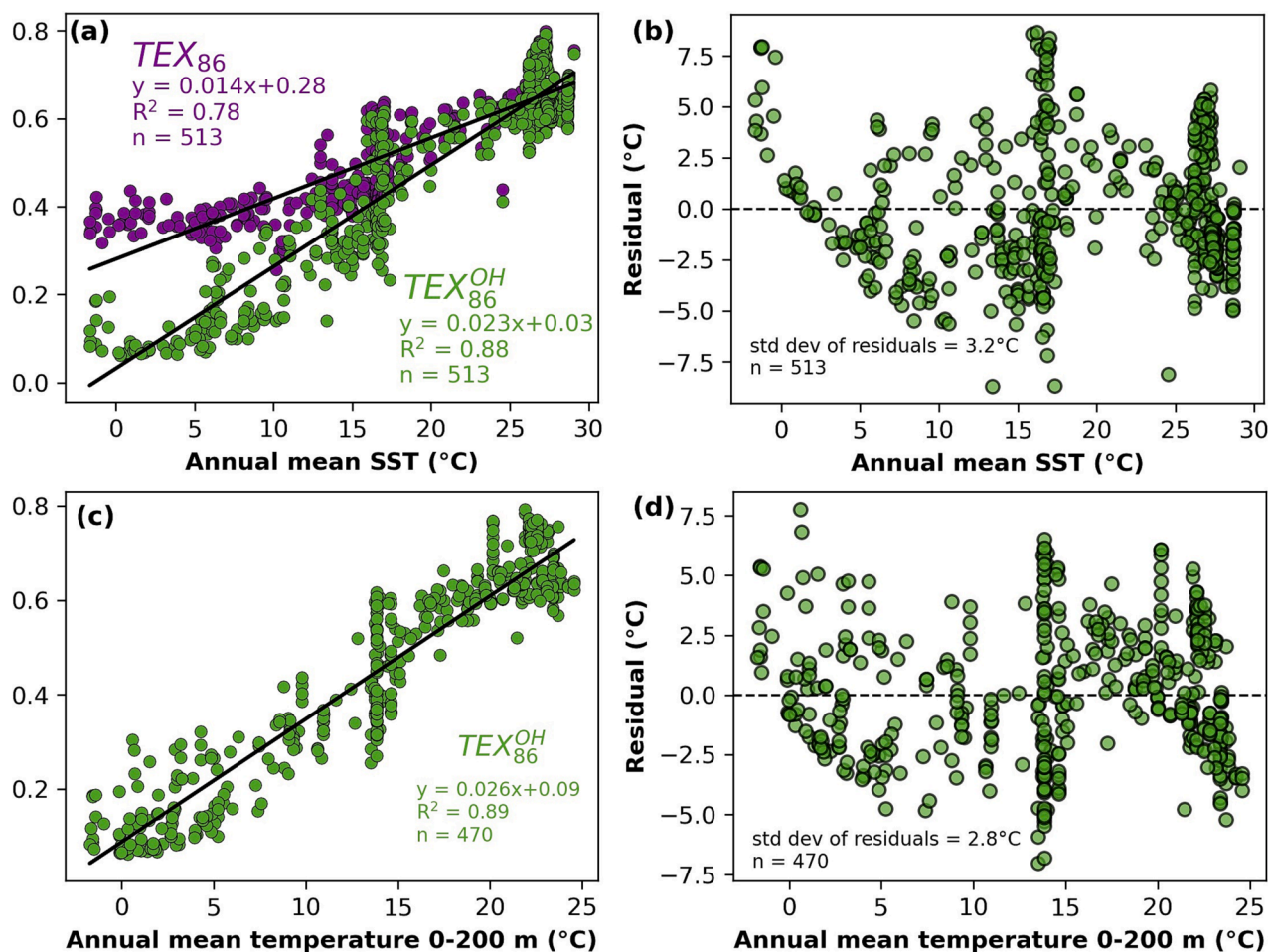


Fig. 7. Correlation of the TEX₈₆^{OH} proxy values for the surface sediments of the NIOZ dataset with (a) annual mean sea SST and (c) 0 – 200 m depth-integrated temperature. Temperature data were obtained from the World Ocean Atlas database. In panel (a) the TEX₈₆– SST correlation is shown for comparison. Panels (b) and (d) show the residual errors calculated for the TEX₈₆^{OH} correlation shown in (a) and (c), respectively.

Fig. 7a, S6). At higher temperatures, OH^C index values are close to TEX₈₆ values because of the low abundance of OH-isoGDGTs at higher SSTs. The OH^C index tends to flatten slightly below 5 °C and above 17 °C, giving it a sigmoidal pattern. Indeed, a polynomial fit with a quadratic function resulted in a slightly better correlation coefficient, similar to other OH-isoGDGT-based proxies (Fig. 6). This observation indicates that the relationships between OH-isoGDGT-based proxies and temperature is likely non-linear, similar to what has been proposed for regular isoGDGTs (cf. Kim et al., 2010).

4.4. Exploring new indices based on OH-isoGDGTs

The strong correlation of OH^C with SST in combination with the results of our PCA, where OH-isoGDGT-0 shows a strong negative correlation with SST, guided us to explore new proxy indices by combining the distributions of OH-isoGDGTs and non-hydroxylated isoGDGTs, based on the idea that both classes of GDGTs are produced primarily by Thaumarchaeota in the ocean (Sollai et al., 2019). We acknowledge that the combination of structurally different OH-isoGDGTs with regular isoGDGTs may lead to biases during diagenesis, and that further research is required to examine potential differences in degradation kinetics of OH-isoGDGTs and isoGDGTs. The OH^C index has the disadvantage that the fractional abundance of OH-isoGDGT-0 is subtracted in the numerator, which results in negative values at SSTs < 12 °C (Fig. 6d). This complicates regressions with non-linear functions. Additionally, since OH-isoGDGT-1 and OH-isoGDGT-2 are often present

at low abundance only and are affected by other parameters than temperature (see above), we decided to include OH-isoGDGT-0 only. Consequently, we used a simple approach, i.e., we added the abundance of OH-isoGDGT-0 to the denominator of the TEX₈₆ and named the new index TEX₈₆^{OH}, i.e., TetraEther index of 86 carbon atoms including OH-isoGDGT-0 (Table 1). Compared to the above discussed dataset, we added back three surface sediments that had OH-isoGDGT-1 or –2 below the detection limit and could therefore not be used to examine OH-isoGDGT distribution patterns. However, they do contain all GDGTs including OH-isoGDGT-0 present in the new TEX₈₆^{OH} index and are thus suitable to examine the environmental controls on this new proxy. Additionally, since OH-isoGDGT-0 abundance is anyway lower in the tropical regions, we also added back 41 surface sediments from regions with annual mean SST > 23 °C that had sufficiently high non-hydroxylated isoGDGT signals but had OH-isoGDGTs below the detection limit. This results in a total of 513 surface sediments used in the analysis of the new TEX₈₆^{OH} index.

Firstly, we investigated the reproducibility of TEX₈₆^{OH} measurements over a period of four years by analyzing our internal standard for this proxy. We observe reproducible values of TEX₈₆^{OH} through time, similar to TEX₈₆ (Figure S2c, S2d). Additionally, as previously mentioned, there may be an analytical bias when utilizing a proxy with both OH-isoGDGTs and isoGDGTs as a result of variations in the degree of in-source dehydration across different instruments in different laboratories. It is necessary to carefully analyze the interlaboratory differences in the extent of in-source dehydration and the ionization efficiencies

between OH-isoGDGTs and regular isoGDGTs. Further, we cross-plotted $\text{TEX}_{86}^{\text{OH}}$ against SST, which resulted in a strong linear correlation ($R^2 = 0.88$, $p < 0.001$ for the NIOZ dataset) (Fig. 7a). When TEX_{86} is compared with the new proxy index $\text{TEX}_{86}^{\text{OH}}$, we observe that $\text{TEX}_{86}^{\text{OH}}$ shows a stronger linear correlation with SST than TEX_{86} (Fig. 7). This is mostly due to a steeper temperature gradient because the new proxy-temperature relationship does not flatten, unlike TEX_{86} , at SSTs $< 15^\circ\text{C}$. Instead, $\text{TEX}_{86}^{\text{OH}}$ remains more or less linearly decreasing with SST up to $\sim 5^\circ\text{C}$ due to the prevalence of OH-isoGDGT-0 at lower temperatures. The overall increased temperature sensitivity may, therefore, potentially improve temperature reconstructions, especially for regions with temperatures $< 15^\circ\text{C}$ (see below).

Since isoGDGTs and OH-isoGDGTs are known to be produced in subsurface waters below the surface (0–30 m), we also correlated the $\text{TEX}_{86}^{\text{OH}}$ proxy with depth-integrated temperatures from 0 to 200 m (see Equation 7 in Kim et al., 2008). Forty-three surface sediments could not be included in this effort, since these locations had insufficient deep temperature data in the WOA database. The resulting ‘sub-surface’ NIOZ dataset ($n = 470$) showed a similar strong correlation ($R^2 = 0.89$) (Fig. 7c, S9a), with a slightly higher slope and intercept compared to the correlation with SST (Table 1). This suggests that the $\text{TEX}_{86}^{\text{OH}}$ proxy may reflect sub-surface rather than surface temperatures, as observed for TEX_{86} (e.g. Wuchter et al., 2005; Huguet et al., 2007).

We compared the residual errors of the new proxy, $\text{TEX}_{86}^{\text{OH}}$ -derived SST (or depth-integrated temperature) with the temperatures from the WOA database (i.e., $\text{TEX}_{86}^{\text{OH}}$ temperature – WOA temperature). The residuals show a sigmoid-like pattern with temperature (Fig. 7b, 7d, S10, S11), suggesting that other factors than temperature could still affect the proxy values. The main regions that showed an overestimation of SST by $\text{TEX}_{86}^{\text{OH}}$ were from the Rhône delta and the Iberian margin, and for some surface sediments from the Antarctic region (for details, see Figure S11). These regions might be influenced by upwelling or changes in

stratification or seasonality which could affect GDGT distributions. The distribution of the OH-isoGDGTs from the Mediterranean might be affected by factors such as water depth, as shown previously for regular isoGDGTs (Kim et al., 2015, 2016; Besseling et al., 2019). To examine this, we removed the Mediterranean surface sediments (including the ones from the Rhône delta and the Iberian margin) and surface sediments with annual mean SST $< 0^\circ\text{C}$. This resulted in slightly improved correlations with SST (R^2 improved from 0.88 to 0.92; Figure S12). Furthermore, a few surface sediments from the Western South Atlantic and Gulf of Mexico showed a strong underestimation of SST ($\sim 8^\circ\text{C}$). The three surface sediments from the Western South Atlantic are from shallow water depths ($< 600\text{ m}$) and might be influenced by the Paraná and the Uruguay River outflow even though BIT values are low.

Finally, we checked for potential differences between $\text{TEX}_{86}^{\text{OH}}$ values from different laboratories as this may prohibit the general application of this new proxy. We calculated $\text{TEX}_{86}^{\text{OH}}$ values for surface sediments from the same 2° grid from the Antarctic region (presumably deposited under similar environmental conditions) but reported by different laboratories (Table 2c). We observe that there is a significant difference between median $\text{TEX}_{86}^{\text{OH}}$ values from different laboratories ($p = 0.006$) at the significance level of 0.05. However, this analysis is based on only a limited number of surface sediments ($n = 11$), so we cannot exclude that this is caused by other factors than interlaboratory differences. We also compared the $\text{TEX}_{86}^{\text{OH}}$ -SST correlations between the NIOZ dataset and the complete global dataset, i.e., the combined dataset from NIOZ and data analyzed in other laboratories (see Figure S9c, S9d) and found a statistically distinguishable slope and intercept at the 5 % significance level (ANCOVA with $p < 0.0001$). Similarly, correlation of the $\text{TEX}_{86}^{\text{OH}}$ with 0–200 m depth integrated temperature showed a strong correlation in the global dataset ($R^2 = 0.90$, $p < 0.001$; Figure S9b), and when compared with the correlation from the NIOZ dataset (see Figure S9a, S9b), showed a statistically distinguishable slope and intercept at the 5

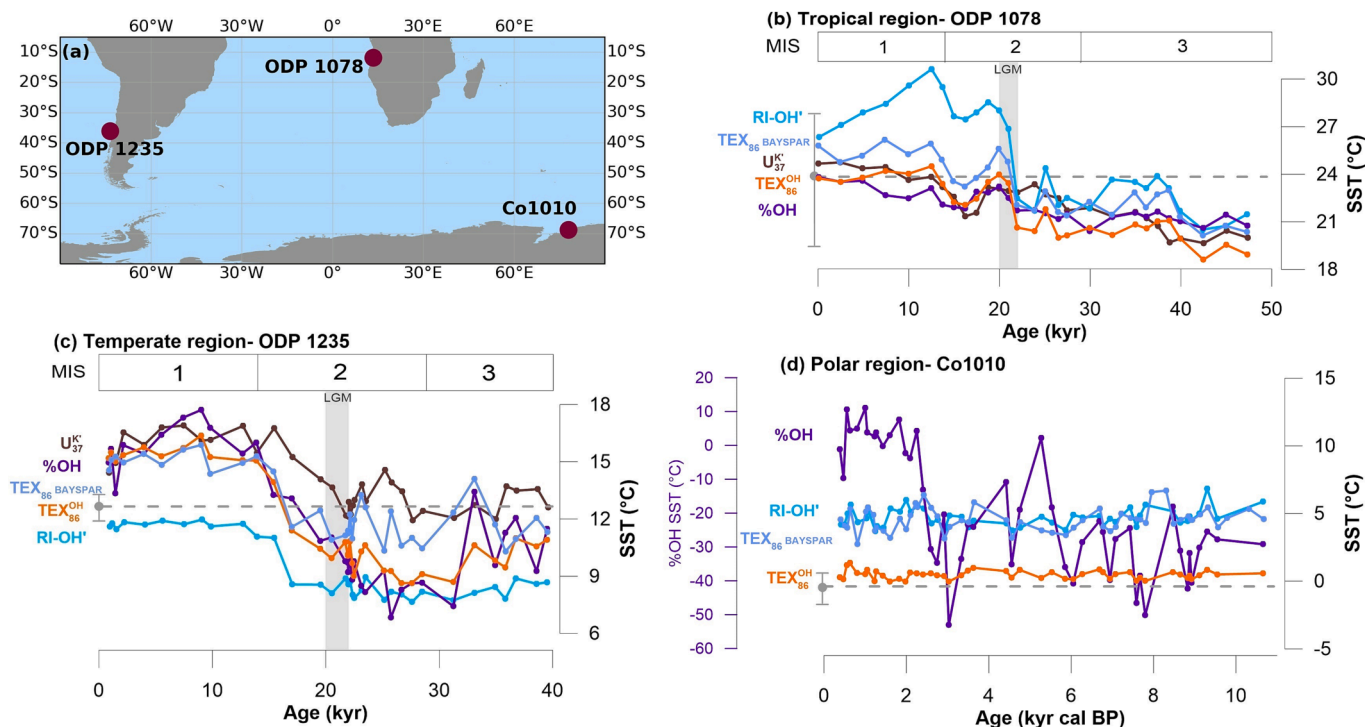


Fig. 8. Application of isoGDGT and OH-isoGDGT based proxies – TEX_{86} BAYSPAR (Tierney and Tingley, 2014, 2015), RI –OH' (Lü et al., 2015), %OH (Huguet et al., 2013) and $\text{TEX}_{86}^{\text{OH}}$ – from this study (based on proxy-SST correlations from the NIOZ dataset). (a) Locations of the sediment cores, (b) ODP 1078 from the Angola margin (Varma et al., 2023), (c) ODP 1235 from the Chilean margin (Varma et al., 2023) and (d) Core Co1010 from Prydz Bay, Antarctica. The SST based on U_{37}^K index is also shown for ODP 1235 and 1078, calculated using the calibration of Müller et al. (1998). The gray symbols with bars and dotted lines denote modern annual mean sea surface temperature (0 m) with seasonal range at each location (Locarnini et al., 2019). MIS = Marine Isotope Stage, LGM = Last Glacial Maximum.

% significance level (ANCOVA with $p = 0.0173$). This observation suggests that potentially small differences may exist between laboratories in measuring $\text{TEX}_{86}^{\text{OH}}$, but it should be noted that we have limited data from other laboratories for comparison. Evidently, a round-robin study on $\text{TEX}_{86}^{\text{OH}}$ is required to resolve potential interlaboratory biases.

4.5. Implications for application of OH-isoGDGT-based proxies

We applied the new $\text{TEX}_{86}^{\text{OH}}$ proxy, together with TEX_{86} as well as previously proposed proxies based on OH-isoGDGTs, on sediment core records from a tropical (Angola margin), a temperate (Chilean margin), and a polar (Prydz Bay) region (Fig. 8; Supplementary Table S2). The isoGDGT and OH-isoGDGT data from the tropics, site ODP 1078 (from the Angola margin), and the temperate region, site ODP 1235 (from the Chilean margin), have previously been published (Varma et al., 2023). Although we are aware that $\text{TEX}_{86}^{\text{OH}}$ likely represents sub-surface temperatures similar to TEX_{86} , in this initial application we are comparing it with U_{37}^{K} , which is also calibrated to SST. For the polar core Co1010, U_{37}^{K} data was not available. As a first simplistic approach, we used the linear correlation between $\text{TEX}_{86}^{\text{OH}}$ and SST (Fig. 7a) as a calibration model.

As expected, we observe that for the sediment core from the tropical Angola margin (Fig. 8b, S13), the new $\text{TEX}_{86}^{\text{OH}}$ record closely matches the $\text{TEX}_{86}^{\text{H}}$ - and TEX_{86} BAYSPAR-derived SST since the OH-isoGDGTs are much less abundant in warm regions of the ocean. The RI–OH' exhibits similar Marine Isotope Stage (MIS) 2 temperatures, but unusually high temperatures at the start of the Holocene compared to the other paleotemperature proxies. However, the RI–OH based temperature estimates are closer to temperatures reconstructed from TEX_{86} and U_{37}^{K} (Figure S13a), which agrees with the conclusion of Lü et al. (2015) that RI–OH works better than RI–OH' in warm regions. Hence, the overall lower abundance of OH-isoGDGTs, especially OH-isoGDGT-0, during warm periods or in tropical regions, along with other influences such as water depth (see above), could have a significant impact on RI–OH' temperature estimates. In contrast, the temperature estimates from %OH and OH^C are in the range of other paleothermometers such as U_{37}^{K} , but show less pronounced differences between glacial and interglacial periods compared to other paleothermometers.

For the ODP 1235 core from the temperate Chilean margin, the $\text{TEX}_{86}^{\text{OH}}$ -derived SSTs for MIS 1 lies within the range of the calibration error of U_{37}^{K} (1.5 °C), while considerably lower SSTs are reconstructed for the colder MIS 2 and 3 periods (Fig. 8c). Similarly, the $\text{TEX}_{86}^{\text{OH}}$ -based temperature record agrees with those obtained with the TEX_{86} BAYSPAR and $\text{TEX}_{86}^{\text{H}}$ for MIS 1, while it records lower temperatures during MIS 2 and 3. This suggests that OH-isoGDGTs may play a significant role in temperate regions, particularly during colder periods when OH-isoGDGT-0 is more abundant, and thus $\text{TEX}_{86}^{\text{OH}}$ yields different temperature estimates compared to TEX_{86} due to its higher sensitivity for lower temperatures. The %OH and OH^C SST records show similar trends to $\text{TEX}_{86}^{\text{OH}}$, although a larger variability is observed for %OH-derived SSTs (Fig. 8c, S13). The RI–OH' reconstructs lower temperatures compared to other proxies, particularly during MIS 1, nonetheless the RI–OH'-derived SST for the most recent datapoint of the record is close to the modern annual mean sea surface temperature range (Fig. 8c). Varma et al. (2023) have reported much lower temperatures estimates of ~ 10 °C for the most recent datapoint for this sediment core using RI–OH'-based on the Fietz et al. (2020) calibration. The new RI–OH'-SST correlation obtained in this study slightly improves the estimated temperatures, although they still do not align with temperature estimates from other proxies in this core. The RI–OH temperature record also shows lower temperatures compared to other proxies and also shows more muted glacial-interglacial temperature variability than RI–OH' (Figure S13), likely because of lower abundance of OH-

isoGDGT-1 and –2 in temperate regions with < 15 °C (Lü et al., 2015).

Interestingly, the polar sediment record (core Co1010) shows $\text{TEX}_{86}^{\text{OH}}$ -derived SST values close to the modern annual mean SST for the past 10 kyr cal BP (Fig. 8d). This is a notable improvement in temperature reconstructions compared to $\text{TEX}_{86}^{\text{H}}$ (Figure S13), which predicts unreasonably high temperatures of ~ 13 °C, as expected (Kim et al., 2010). The RI–OH', RI–OH and TEX_{86} BAYSPAR give lower temperature estimates than $\text{TEX}_{86}^{\text{H}}$, but the absolute SST values are still much higher than the modern SST value at this location (Fig. 8d, S13). However, the OH^C reconstructs lower temperatures (at ~ -5 °C) compared to modern annual mean SST (Figure S13). The %OH temperatures in this record shows unreasonable temperatures ranging from –53 to 11 °C, which suggests it is likely not a useful paleothermometer in the Antarctic region. Interestingly, the isoGDGT-0/cren ratio is > 2 for sediments from 0 to ~ 2.5 kyr cal BP, potentially indicating a contribution of methanogenic Euryarchaeota (Blaga et al., 2009). However, this does not appear to impact any of the paleothermometers, possibly apart from a higher %OH. Overall, the Co1010 record shows the potential of $\text{TEX}_{86}^{\text{OH}}$ to reconstruct temperatures in polar and also temperate regions much better than TEX_{86} or other OH-isoGDGT-based proxies.

5. Conclusions

We have substantially increased the geographic coverage of the OH-isoGDGT surface sediment data in the global ocean compared to previous studies. PCA results indicate a strong temperature signal in the OH-isoGDGT distribution, especially for OH-isoGDGT-0. However, our analysis also shows that OH-isoGDGT-1 and –2 could be affected by water depth, especially in regions with annual mean SST > 25 °C. This dependency with water depth appears to have an impact on the RI–OH' and RI–OH indices, resulting in substantial deviations in temperature estimates in warm temperature regions. We observe discrepancies among laboratories when using proxies based on regular isoGDGTs and OH-isoGDGTs, but the effect may be less significant on proxies that are solely based on the abundances of OH-isoGDGTs. This observation necessitates a round-robin study to evaluate the causes of the differences between laboratories in analyzing OH-isoGDGTs and isoGDGTs.

We explored a new proxy index $\text{TEX}_{86}^{\text{OH}}$, by introducing the abundance of OH-isoGDGT-0 in the denominator of the TEX_{86} index. This new $\text{TEX}_{86}^{\text{OH}}$ index shows substantial improvement in its correlation with SST (or with 0–200 m depth-integrated temperature) compared to TEX_{86} and the overall increased temperature sensitivity of $\text{TEX}_{86}^{\text{OH}}$ may improve the temperature estimates, particularly in cold regions with temperatures < 15 °C. Our initial application of this new proxy index to downcore sediments shows promising results especially in temperate and polar regions. Further work is required on both a regional and global scale to properly test and calibrate the new $\text{TEX}_{86}^{\text{OH}}$.

Data availability

Research data has been supplied via the repositories: <https://dataportal.nioz.nl/doi/10.25850/nioz/7b.b.6f>, <https://dataportal.nioz.nl/doi/10.25850/nioz/7b.b.7f> and <https://doi.org/10.1594/PANGAEA.957090>. The data for surface sediments and sediment core Co1010 is also uploaded in PANGAEA.

Declaration of competing interest

The authors declare that they have no known competing financial interests or personal relationships that could have appeared to influence the work reported in this paper.

Acknowledgement

We thank Annelieke Mets, Monique Verweij and Denise Dorhout for analytical support. We are grateful to the individuals who supplied or extracted the surface sediments for previous studies and utilized in this study: Marijke de Bar, Julie Lattaud, Hartmut Schulz, Cindy De Jonge, Matthias Moros, Julian Hartman, Furu Mienis, Geert-Jan A. Brummer, Claudia Zell, Lisa Warden, Gabriella Weiss, Veronica Willmott, Jan-Berend W. Stuut, Barbara Donner, Jochen Knies and Andreas Lückge. This research used sediments provided by the International Ocean Discovery Program (IODP). This work was carried out under the program of the Netherlands Earth System Science Centre (NESSC), financially supported by the Ministry of Education, Culture and Science (OCW) through grant 024.002.001 to JSSD and SS. This project has received funding from the European Union's Horizon 2020 research and innovation program under the Marie Skłodowska-Curie, grant agreement No 847504.

Appendix A. Supplementary material

The supplementary materials contain two data files used in the study. The details pertaining to all surface sediments analyzed in this study along with compilation of the previously published hydroxylated isoprenoidal GDGT data as discussed in this study is provided in an Excel sheet as Supplementary Table S1. The temperature records for three sediment cores discussed in the study Co1010, ODP Site 1235 and ODP Site 1078 is provided in another Excel sheet Supplementary Table S2.

Supplementary material to this article can be found online at <http://doi.org/10.1016/j.gca.2023.12.019>.

References

- Allaart, L., Müller, J., Schomacker, A., Rydningen, T.A., Håkansson, L., Kjellman, S.E., Mollenhauer, G., Forwick, M., 2020. Late Quaternary glacier and sea-ice history of northern Wijdefjorden, Svalbard. *Boreas* 49, 417–437.
- Bale, N.J., Villanueva, L., Hopmans, E.C., Schouten, S., Sinninghe Damsté, J.S., 2013. Different seasonality of pelagic and benthic \thaumarchaeota in the North Sea. *Biogeosciences* 10, 7195–7206.
- Bale, N.J., Villareal, T.A., Hopmans, E.C., Brussaard, C.P.D., Besseling, M., Dorhout, D., Sinninghe Damsté, J.S., Schouten, S., 2018. C5 glycolipids of heterocystous cyanobacteria track symbiont abundance in the diatom *Hemiaulus hauckii* across the tropical North Atlantic. *Biogeosciences* 15, 1229–1241.
- Bale, N.J., Palatinszky, M., Rijpstra, W.I.C., Herbold, C.W., Wagner, M., Sinninghe Damsté, J.S., 2019. Membrane lipid composition of the moderately thermophilic ammonia-oxidizing archaeon “*Candidatus Nitrosotenuis uzonensis*” at different growth temperatures. *Appl. Environ. Microbiol.* 85.
- Bale, N.J., Ding, S., Hopmans, E.C., Arts, M.G.L., Villanueva, L., Boschman, C., Haas, A.F., Schouten, S., Sinninghe Damsté, J.S., 2021. Lipidomics of environmental microbial communities. I: Visualization of component distributions using untargeted analysis of high-resolution mass spectrometry data. *Front. Microbiol.* 12, 659302.
- Berg, S., Wagner, B., Cremer, H., Leng, M.J., Melles, M., 2010. Late Quaternary environmental and climate history of Rauer Group, East Antarctica. *Palaeogeogr. Palaeoclimatol. Palaeoecol.* 297, 201–213.
- Berg, S., Jivcov, S., Kusch, S., Kuhn, G., Wacker, L., Rethemeyer, J., 2020. Compound-specific radiocarbon analysis of (sub-)Antarctic coastal marine sediments—potential and challenges for chronologies. *Paleoceanogr. Paleoclimatology* 35.
- Besseling, M.A., Hopmans, E.C., Koenen, M., van der Meer, M.T.J., Vreugdenhil, S., Schouten, S., Sinninghe Damsté, J.S., Villanueva, L., 2019. Depth-related differences in archaeal populations impact the isoprenoid tetraether lipid composition of the Mediterranean Sea water column. *Org. Geochem.* 135, 16–31.
- Besseling, M.A., Hopmans, E.C., Bale, N.J., Schouten, S., Sinninghe Damsté, J.S., Villanueva, L., 2020. The absence of intact polar lipid-derived GDGTs in marine waters dominated by Marine Group II: Implications for lipid biosynthesis in Archaea. *Sci. Rep.* 10.
- Blaga, C.I., Reichert, G.J., Heiri, O., Sinninghe Damsté, J.S., 2009. Tetraether membrane lipid distributions in water-column particulate matter and sediments: A study of 47 European lakes along a north-south transect. *J. Paleolimnol.* 41, 523–540.
- Bligh, E.G., Dyer, W.J., 1959. A rapid method of total lipid extraction and purification. *Can. J. Biochem. Physiol.* 37, 911–917.
- Brassell, S.C., 2014. Climatic influences on the Paleogene evolution of alkenones. *Paleoceanography* 29, 255–272.
- Brassell, S.C., Eglinton, G., Marlowe, I.T., Pflaumann, U., Sarnthein, M., 1986. Molecular stratigraphy: A new tool for climatic assessment. *Nature* 320, 129–133.
- Davtian, N., Ménot, G., Fagault, Y., Bard, E., 2019. Western Mediterranean Sea paleothermometry over the Last Glacial Cycle based on the novel RI-OH index. *Paleoceanogr. Paleoclimatology* 34, 616–634.
- Davtian, N., Bard, E., Darfeuille, S., Ménot, G., Rostek, F., 2021. The novel hydroxylated tetraether index RI-OH' as a sea surface temperature proxy for the 160–45 ka BP period off the Iberian margin. *Paleoceanogr. Paleoclimatology* 36, 1–34.
- Davtian, N., Bard, E., 2023. A new view on abrupt climate changes and the bipolar seesaw based on paleotemperatures from Iberian Margin sediments. *Proc. Natl. Acad. Sci.* 120, e2209558120.
- de Bar, M.W., Weiss, G., Yildiz, C., Rampen, S.W., Lattaud, J., Bale, N.J., Mienis, F., Brummer, G.J.A., Schulz, H., Rush, D., Kim, J.H., Donner, B., Knies, J., Lückge, A., Stuut, J.B.W., Sinninghe Damsté, J.S., Schouten, S., 2020. Global temperature calibration of the Long chain Diol Index in marine surface sediments. *Org. Geochem.* 142, 103983.
- De Jonge, C., Stadnitskaia, A., Hopmans, E.C., Cherkashov, G., Fedotov, A., Streletskaia, I.D., Vasiliev, A.A., Sinninghe Damsté, J.S., 2015. Drastic changes in the distribution of branched tetraether lipids in suspended matter and sediments from the Yenisei River and Kara Sea (Siberia): Implications for the use of brGDGT-based proxies in coastal marine sediments. *Geochim. Cosmochim. Acta* 165, 200–225.
- de Leeuw, J. W., v.d. Meer, F. W., Rijpstra, W. I. C. and Schenck, P. A. 1980. On the occurrence and structural identification of long chain unsaturated ketones and hydrocarbons in sediments. *Phys. Chem. Earth* 12, 211–217.
- Elling, F.J., Könneke, M., Lipp, J.S., Becker, K.W., Gagen, E.J., Hinrichs, K.U., 2014. Effects of growth phase on the membrane lipid composition of the thaumarchaeon *Nitrosopumilus maritimus* and their implications for archaeal lipid distributions in the marine environment. *Geochim. Cosmochim. Acta* 141, 579–597.
- Elling, F.J., Könneke, M., Mußmann, M., Greve, A., Hinrichs, K.U., 2015. Influence of temperature, pH, and salinity on membrane lipid composition and TEX₈₆ of marine planktonic thaumarchaeal isolates. *Geochim. Cosmochim. Acta* 171, 238–255.
- Elling, F.J., Könneke, M., Nicol, G.W., Stieglmeier, M., Bayer, B., Spieck, E., de la Torre, J.R., Becker, K.W., Thomm, M., Prosser, J.I., Herndl, G.J., Schleper, C., Hinrichs, K.U., 2017. Chemotaxonomic characterisation of the thaumarchaeal lipidome. *Environ. Microbiol.* 19, 2681–2700.
- Evans, T.W., Coffinet, S., Könneke, M., Lipp, J.S., Becker, K.W., Elvert, M., Heuer, V., Hinrichs, K.U., 2019. Assessing the carbon assimilation and production of benthic archaeal lipid biomarkers using lipid-RIP. *Geochim. Cosmochim. Acta* 265, 431–442.
- Fallet, U., Castañeda, I.S., Henry-Edwards, A., Richter, T.O., Boer, W., Schouten, S., Brummer, G.J., 2012. Sedimentation and burial of organic and inorganic temperature proxies in the Mozambique Channel, SW Indian Ocean. *Deep. Res. Part I Oceanogr. Res. Pap.* 59, 37–53.
- Fietz, S., Huguet, C., Rueda, G., Hambach, B., Rosell-Melé, A., 2013. Hydroxylated isoprenoidal GDGTs in the Nordic Seas. *Mar. Chem.* 152, 1–10.
- Fietz, S., Ho, S.L., Huguet, C., Rosell-Melé, A., Martínez-García, A., 2016. Appraising GDGT-based seawater temperature indices in the Southern Ocean. *Org. Geochem.* 102, 93–105.
- Fietz, S., Ho, S.L., Huguet, C., 2020. Archaeal membrane lipid-based paleothermometry for applications in polar oceans. *Oceanography* 33, 105–114.
- Gabriel, J.L., Chong, P.L.G., 2000. Molecular modeling of archaeobacterial bipolar tetraether lipid membranes. *Chem. Phys. Lipids* 105, 193–200.
- García H., Weathers K. W., Paver C. R., Smolyar I., Boyer T. P., Locarnini R. A., Zweng M. M., Mishonov A. V., Baranova O. K., Seidov D. and Reagan J. R. 2018. World Ocean Atlas 2018. Volume 4: Dissolved Inorganic Nutrients (phosphate, nitrate and nitrate +nitrite, silicate).
- Heaton, T.J., Blauuw, M., Blackwell, P.G., Bronk, R.C., Reimer, P.J., Scott, E.M., 2020. The IntCal20 Approach to Radiocarbon Calibration Curve Construction: A New Methodology Using Bayesian Splines and Errors-in-Variables. *Radiocarbon* 62, 821–863.
- Herndl, G.J., Reinthaler, T., Teira, E., Van Aken, H., Veth, C., Pernthaler, A., Pernthaler, J., 2005. Contribution of Archaea to total prokaryotic production in the deep Atlantic Ocean. *Appl. Environ. Microbiol.* 71, 2303–2309.
- Ho, S.L., Laepple, T., 2016. Flat meridional temperature gradient in the early Eocene in the subsurface rather than surface ocean. *Nat. Geosci.* 9, 606–610.
- Ho, S.L., Mollenhauer, G., Fietz, S., Martínez-García, A., Lamy, F., Rueda, G., Schipper, K., Méheust, M., Rosell-Melé, A., Stein, R., Tiedemann, R., 2014. Appraisal of TEX₈₆ and TEX₈₆ thermometries in subpolar and polar regions. *Geochim. Cosmochim. Acta* 131, 213–226.
- Holzheimer, M., Sinninghe Damsté, J.S., Schouten, S., Havenith, R.W.A., Cunha, A.V., Minnaard, A.J., 2021. Total Synthesis of the Alleged Structure of Crenarchaeol Enables Structure Revision. *Angew. Chemie Int. Ed.* 60, 17504–17513.
- Hopmans, E.C., Weijers, J.W.H., Schefuß, E., Herfort, L., Sinninghe Damsté, J.S., Schouten, S., 2004. A novel proxy for terrestrial organic matter in sediments based on branched and isoprenoid tetraether lipids. *Earth Planet. Sci. Lett.* 224, 107–116.
- Hopmans, E.C., Schouten, S., Sinninghe Damsté, J.S., 2016. The effect of improved chromatography on GDGT-based paleoproxies. *Org. Geochem.* 93, 1–6.
- Huber, M. 2010. Why improving molecular and isotopic proxy paleoclimate records is the most important problem in science today: A climate modeling perspective. In: Gordon Research Conference. Holderness, NH, USA.
- Huguet, C., Schimmelmann, A., Thunell, R., Lourens, L.J., Sinninghe Damsté, J.S., Schouten, S., 2007. A study of the TEX₈₆ paleothermometer in the water column and sediments of the Santa Barbara Basin, California. *Paleoceanography* 22, 3203.
- Huguet, C., Fietz, S., Rosell-Melé, A., 2013. Global distribution patterns of hydroxy glycerol dialkyl glycerol tetraethers. *Org. Geochem.* 57, 107–118.
- Huguet, C., Fietz, S., Rosell-Melé, A., Daura, X., Costenaro, L., 2017. Molecular dynamics simulation study of the effect of glycerol dialkyl glycerol tetraether hydroxylation on membrane thermostability. *Biochim. Biophys. Acta - Biomembr.* 1859, 966–974.
- Hurley, S.J., Elling, F.J., Könneke, M., Buchwald, C., Wankel, S.D., Santoro, A.E., Lipp, J. S., Hinrichs, K.U., Pearson, A., 2016. Influence of ammonia oxidation rate on

- thaumarchaeal lipid composition and the TEX₈₆ temperature proxy. *Proc. Natl. Acad. Sci. U. S. A.* 113, 7762–7767.
- Hurley, S.J., Lipp, J.S., Close, H.G., Hinrichs, K.U., Pearson, A., 2018. Distribution and export of isoprenoid tetraether lipids in suspended particulate matter from the water column of the Western Atlantic Ocean. *Org. Geochem.* 116, 90–102.
- Inglis, G.N., Farnsworth, A., Lunt, D., Foster, G.L., Hollis, C.J., Pagani, M., Jardine, P.E., Pearson, P.N., Markwick, P., Galsworthy, A.M.J., Raynham, L., Taylor, K.W.R., Pancost, R.D., 2015. Descent toward the Icehouse: Eocene sea surface cooling inferred from GDGT distributions. *Paleoceanography* 30, 1000–1020.
- Kaiser, J., Arz, H.W., 2016. Sources of sedimentary biomarkers and proxies with potential paleoenvironmental significance for the Baltic Sea. *Cont. Shelf Res.* 122, 102–119.
- Kang, S., Shin, K.H., Kim, J.H., 2017. Occurrence and distribution of hydroxylated isoprenoid glycerol dialkyl glycerol tetraethers (OH-GDGTs) in the Han River system, South Korea. *Acta Geochim.* 36, 367–369.
- Karner, M.B., Delong, E.F., Karl, D.M., 2001. Archaeal dominance in the mesopelagic zone of the Pacific Ocean. *Nature* 409, 507–510.
- Kim, J.H., Schouten, S., Hopmans, E.C., Donner, B., Sinninghe Damsté, J.S., 2008. Global sediment core-top calibration of the TEX₈₆ paleothermometer in the ocean. *Geochim. Cosmochim. Acta* 72, 1154–1173.
- Kim, J.H., van der Meer, J., Schouten, S., Helmke, P., Willmott, V., Sangiorgi, F., Koç, N., Hopmans, E.C., Sinninghe Damsté, J.S., 2010. New indices and calibrations derived from the distribution of crenarchaeal isoprenoid tetraether lipids: Implications for past sea surface temperature reconstructions. *Geochim. Cosmochim. Acta* 74, 4639–4654.
- Kim, J.H., Schouten, S., Rodrigo-Gámiz, M., Rampen, S., Marino, G., Huguët, C., Helmke, P., Buscail, R., Hopmans, E.C., Pross, J., Sangiorgi, F., Middelburg, J.B.M., Sinninghe Damsté, J.S., 2015. Influence of deep-water derived isoprenoid tetraether lipids on the TEX₈₆ paleothermometer in the Mediterranean Sea. *Geochim. Cosmochim. Acta* 150, 125–141.
- Kim, J.H., Villanueva, L., Zell, C., Sinninghe Damsté, J.S., 2016. Biological source and provenance of deep-water derived isoprenoid tetraether lipids along the Portuguese continental margin. *Geochim. Cosmochim. Acta* 172, 177–204.
- Könneke, M., Bernhard, A.E., De La Torre, J.R., Walker, C.B., Waterbury, J.B., Stahl, D. A., 2005. Isolation of an autotrophic ammonia-oxidizing marine archaeon. *Nature* 437, 543–546.
- Kremer, A., Stein, R., Fahl, K., Ji, Z., Yang, Z., Wiers, S., Matthiessen, J., Forwick, M., Löwemark, L., O'Regan, M., Chen, J., Snowball, L., 2018. Changes in sea ice cover and ice sheet extent at the Yermak Plateau during the last 160 ka – Reconstructions from biomarker records. *Quat. Sci. Rev.* 182, 93–108.
- Lamping, N., Müller, J., Hefter, J., Mollenhauer, G., Haas, C., Shi, X., Vorrath, M.-E., Lohmann, G., Hillenbrand, C.-D., 2021. Evaluation of lipid biomarkers as proxies for sea ice and ocean temperatures along the Antarctic continental margin. *Clim. past* 17, 2305–2326.
- Lattaud, J., Kirkels, F., Peterse, F., Freymond, C.V., Eglinton, T.I., Hefter, J., Mollenhauer, G., Balzano, S., Villanueva, L., Van Der Meer, M.T.J., Hopmans, E.C., Sinninghe Damsté, J.S., Schouten, S., 2018. Long-chain diols in rivers: Distribution and potential biological sources. *Biogeosciences* 15, 4147–4161.
- Liu, L., Guan, H., Xu, L., Sun, Z., Wu, N., 2022. Paleoclimate records of the middle Okinawa trough since the middle Holocene: Modulation of the low-latitude climate. *Front. Earth Sci.* 10, 1–13.
- Liu, R., Han, Z., Zhao, J., Haifeng, Z., Li, D., Ren, J., Pan, J., Haisheng, Z., 2020. Distribution and source of glycerol dialkyl glycerol tetraethers (GDGTs) and the applicability of GDGT-based temperature proxies in surface sediments of Prydz Bay, East Antarctica. *Polar Res.* 39, 1–15.
- Liu, X.-L., Lipp, J.S., Simpson, J.H., Lin, Y.S., Summons, R.E., Hinrichs, K.U., 2012a. Mono- and dihydroxyl glycerol dibiphytanyl glycerol tetraethers in marine sediments: Identification of both core and intact polar lipid forms. *Geochim. Cosmochim. Acta* 89, 102–115.
- Liu, X.-L., Summons, R.E., Hinrichs, K.U., 2012b. Extending the known range of glycerol ether lipids in the environment: Structural assignments based on tandem mass spectral fragmentation patterns. *Rapid Commun. Mass Spectrom.* 26, 2295–2302.
- Lo, L., Belt, S.T., Lattaud, J., Friedrich, T., Zeeden, C., Schouten, S., Smik, L., Timmermann, A., Cabedo-Sanz, P., Huang, J.J., Zhou, L., Ou, T.H., Chang, Y.P., Wang, L.C., Chou, Y.M., Shen, C.C., Chen, M., Te, W.K.Y., Song, S.R., Fang, T.H., Gorbarenko, S.A., Wang, W.L., Lee, T.Q., Elderfield, H., Hodell, D.A., 2018. Precession and atmospheric CO₂ modulated variability of sea ice in the central Okhotsk Sea since 130,000 years ago. *Earth Planet. Sci. Lett.* 488, 36–45.
- Locarnini, R. A., Mishonov, A. V., Baranova, O. K., Boyer, T. P., Zweng, M. M., Garcia, H. E., Reagan, J. R., Seidov, D., Weathers, K. W., Paver, C. R. and Smolyar, I. V. 2019. *World Ocean Atlas 2018, Volume 1: Temperature*. A. Mishonov, Technical Editor.
- Lü, X., Liu, X.L., Elling, F.J., Yang, H., Xie, S., Song, J., Li, X., Yuan, H., Li, N., Hinrichs, K. U., 2015. Hydroxylated isoprenoid GDGTs in Chinese coastal seas and their potential as a paleotemperature proxy for mid-to-low latitude marginal seas. *Org. Geochem.* 89–90, 31–43.
- Lü, X., Chen, J., Han, T., Yang, H., Wu, W., Ding, W., Hinrichs, K.U., 2019. Origin of hydroxyl GDGTs and regular isoprenoid GDGTs in suspended particulate matter of Yangtze River Estuary. *Org. Geochem.* 128, 78–85.
- Man, Y., Fan, J., Huang, M., Yang, H., 2023. An unusual occurrence of hydroxylated isoprenoid GDGTs in forest soils. *Org. Geochem.* 177, 104540.
- Morçillo-Montalbá, L., Rodrigo-Gámiz, M., Martínez-Ruiz, F., Ortega-Huertas, M., Schouten, S., Sinninghe Damsté, J.S., 2021. Rapid Climate Changes in the Westernmost Mediterranean (Alboran Sea) Over the Last 35 kyr: New Insights From Four Lipid Paleothermometers (U₃₇^K, TEX₈₆^H, RI-OH^H, and LDI). *Paleoceanogr. Paleoclimatology* 36.
- Müller, P.J., Kirst, G., Ruhland, G., Von Storch, I., Rosell-Melé, A., 1998. Calibration of the alkenone paleotemperature index UK'37 based on core-tops from the eastern South Atlantic and the global ocean (60°N–60°S). *Geochim. Cosmochim. Acta* 62, 1757–1772.
- O'Brien, C.L., Robinson, S.A., Pancost, R.D., Sinninghe Damsté, J.S., Schouten, S., Lunt, D.J., Alsenz, H., Bornemann, A., Bottini, C., Brassell, S.C., Farnsworth, A., Forster, A., Huber, B.T., Inglis, G.N., Jenkyns, H.C., Linnert, C., Littler, K., Markwick, P., McAnena, A., Mutterlose, J., Naafs, B.D.A., Püttmann, W., Sluijs, A., van Helmond, N.A.G.M., Vellekoop, J., Wagner, T., Wrobel, N.E., 2017. Cretaceous sea-surface temperature evolution: Constraints from TEX₈₆ and planktonic foraminiferal oxygen isotopes. *Earth-Science Rev.* 172, 224–247.
- Peterse, F., Kim, J.H., Schouten, S., Kristensen, D.K., Koç, N., Sinninghe Damsté, J.S., 2009. Constraints on the application of the MBT/CBT paleothermometer at high latitude environments (Svalbard, Norway). *Org. Geochem.* 40, 692–699.
- Polik, C.A., Elling, F.J., Pearson, A., 2018. Impacts of Paleocology on the TEX₈₆ Sea Surface Temperature Proxy in the Pliocene-Pleistocene Mediterranean Sea. *Paleoceanogr. Paleoclimatology* 33, 1472–1489.
- Prahl, F.G., Wakeham, S.G., 1987. Calibration of unsaturation patterns in long-chain ketone compositions for paleotemperature assessment. *Nature* 330, 367–369.
- Rattanasriampipong, R., Zhang, Y.G., Pearson, A., Hedlund, B.P., Zhang, S., 2022. Archaeal lipids trace ecology and evolution of marine ammonia-oxidizing archaea. *Proc. Natl. Acad. Sci. U. S. A.* 119, 1–10.
- Rinke, C., Chuvochina, M., Mussig, A.J., Chaumeil, P.A., Davin, A.A., Waite, D.W., Whitman, W.B., Parks, D.H., Hugenholtz, P., 2021. A standardized archaeal taxonomy for the Genome Taxonomy Database. *Nat. Microbiol.* 6, 946–959.
- Rosell-Melé, A., Bard, E., Emeis, K.C., Grimalt, J.O., Müller, P., Schneider, R., Bouloubassi, I., Epstein, B., Fahl, K., Fluegge, A., Freeman, K., Goñi, M., Güntner, U., Hartz, D., Hellebust, S., Herbert, T., Ikehara, M., Ishiwatari, R., Kawamura, K., Kenig, F., De Leeuw, J., Lehman, S., Mejanella, L., Ohkouchi, N., Pancost, R.D., Pelejero, C., Prahl, F., Quinn, J., Rontani, J.F., Rostek, F., Rullkötter, J., Sachs, J., Blanz, T., Sawada, K., Schulz-Bull, D., Sikkes, E., Sonzogni, C., Ternois, Y., Versteegh, G., Volkman, J.K., Wakeham, S., 2001. Precision of the current methods to measure the alkenone proxy U₃₇^K and absolute alkenone abundance in sediments: Results of an interlaboratory comparison study. *Geochemistry, Geophys. Geosystems* 2, 1046.
- Schouten, S., Hopmans, E.C., Schefuß, E., Sinninghe Damsté, J.S., 2002. Distributional variations in marine crenarchaeotal membrane lipids: A new tool for reconstructing ancient sea water temperatures? *Earth Planet. Sci. Lett.* 204, 265–274.
- Schouten, S., Hopmans, E.C., Van Der Meer, J., Mets, A., Bard, E., Bianchi, T.S., Diefendorf, A., Escala, M., Freeman, K.H., Furukawa, Y., Huguët, C., Ingalls, A., Ménot-Combes, G., Nederbragt, A.J., Oba, M., Pearson, A., Pearson, E.J., Rosell-Melé, A., Schaeffer, P., Shah, S.R., Shanahan, T.M., Smith, R.W., Smittenberg, R., Talbot, H.M., Uchida, M., Van Mooy, B.A.S., Yamamoto, M., Zhang, Z., Sinninghe Damsté, J.S., 2009. An interlaboratory study of TEX₈₆ and BIT analysis using high-performance liquid chromatography-mass spectrometry. *Geochemistry, Geophys. Geosystems* 10, 1–13.
- Schouten, S., Hopmans, E.C., Rosell-Melé, A., Pearson, A., Adam, P., Bauersachs, T., Bard, E., Bernasconi, S.M., Bianchi, T.S., Brocks, J.J., Carlson, L.T., Castañeda, I.S., Derenne, S., Selver, A.D., Dutta, K., Eglinton, T., Fosse, C., Galy, V., Grice, K., Hinrichs, K.U., Huang, Y., Huguët, A., Huguët, C., Hurley, S., Ingalls, A., Jia, G., Keely, B., Knappy, C., Kondo, M., Krishnan, S., Lincoln, S., Lipp, J., Mangelsdorf, K., Martínez-García, A., Ménot, G., Mets, A., Mollenhauer, G., Ohkouchi, N., Ossebaer, J., Pagani, M., Pancost, R.D., Pearson, E.J., Peterse, F., Reichert, G.J., Schaeffer, P., Schmitt, G., Schwark, L., Shah, S.R., Smith, R.W., Smittenberg, R.H., Summons, R.E., Takano, Y., Talbot, H.M., Taylor, K.W.R., Tarozo, R., Uchida, M., Van Dongen, B.E., Van Mooy, B.A.S., Wang, J., Warren, C., Weijers, J.W.H., Werne, J.P., Woltering, M., Xie, S., Yamamoto, M., Yang, H., Zhang, C.L., Zhang, Y., Zhao, M., Sinninghe Damsté, J.S., 2013a. An interlaboratory study of TEX₈₆ and BIT analysis of sediments, extracts, and standard mixtures. *Geochemistry, Geophys. Geosystems* 14, 5263–5285.
- Schouten, S., Hopmans, E.C., Sinninghe Damsté, J.S., 2013b. The organic geochemistry of glycerol dialkyl glycerol tetraether lipids: A review. *Org. Geochem.* 54, 19–61.
- Schulz, H., Lückge, A., Emeis, K.C., Mackensen, A., 2011. Variability of Holocene to Late Pleistocene Zambezi riverine sedimentation at the upper continental slope off Mozambique, 15°–21°S. *Mar. Geol.* 286, 21–34.
- Sinninghe Damsté, J.S., 2016. Spatial heterogeneity of sources of branched tetraethers in shelf systems: The geochemistry of tetraethers in the Berau River delta (Kalimantan, Indonesia). *Geochim. Cosmochim. Acta* 186, 13–31.
- Sinninghe Damsté, J.S., Schouten, S., Hopmans, E.C., Van Duin, A.C.T., Geenevasen, J.A. J., 2002. Crenarchaeol: The characteristic core glycerol dibiphytanyl glycerol tetraether membrane lipid of cosmopolitan pelagic crenarchaeota. *J. Lipid Res.* 43, 1641–1651.
- Sinninghe Damsté, J.S., Rijpstra, W.I.C., Hopmans, E.C., Jung, M.Y., Kim, J.G., Rhee, S. K., Stieglmeier, M., Schleper, C., 2012. Intact polar and core glycerol dibiphytanyl glycerol tetraether lipids of group I.1a and I.1b Thaumarchaeota in soil. *Appl. Environ. Microbiol.* 78, 6866–6874.
- Sinninghe Damsté, J.S., Warden, L.A., Berg, C., Jürgens, K., Moros, M., 2022a. Evaluation of the distributions of hydroxylated glycerol dibiphytanyl glycerol tetraethers (GDGTs) in Holocene Baltic Sea sediments for reconstruction of sea surface temperature: The effect of changing salinity. *Clim. past* 18, 2271–2288.
- Sinninghe Damsté, J.S., Weber, Y., Zopfi, J., Lehmann, M.F., Niemann, H., 2022b. Distributions and sources of isoprenoid GDGTs in Lake Lugano and other central European (peri-)alpine lakes: Lessons for their use as paleotemperature proxies. *Quat. Sci. Rev.* 277, 107352.
- Smith, M., De Deckker, P., Rogers, J., Brocks, J., Hope, J., Schmidt, S., Lopes dos Santos, R., Schouten, S., 2013. Comparison of U₃₇^K, TEX₈₆^H and LDI temperature

- proxies for reconstruction of south-east Australian ocean temperatures. *Org. Geochem.* 64, 94–104.
- Sollai, M., Villanueva, L., Hopmans, E.C., Reichart, G.J., Sinninghe Damsté, J.S., 2019. A combined lipidomic and 16S rRNA gene amplicon sequencing approach reveals archaeal sources of intact polar lipids in the stratified Black Sea water column. *Geobiology* 17, 91–109.
- Sturt, H.F., Summons, R.E., Smith, K., Elvert, M., Hinrichs, K.U., 2004. Intact polar membrane lipids in prokaryotes and sediments deciphered by high-performance liquid chromatography/electrospray ionization multistage mass spectrometry—new biomarkers for biogeochemistry and microbial ecology. *Rapid Commun. Mass Spectrom.* 18, 617–628.
- Taylor, K.W.R., Huber, M., Hollis, C.J., Hernandez-Sanchez, M.T., Pancost, R.D., 2013. Re-evaluating modern and Palaeogene GDGT distributions: Implications for SST reconstructions. *Glob. Planet. Change* 108, 158–174.
- Tierney, J.E., 2013. Biomarker-based inferences of past climate: The TEX₈₆ paleotemperature proxy. *Treatise on Geochemistry*: 2nd Ed. 12, 379–393.
- Tierney, J.E., Tingley, M.P., 2014. A Bayesian, spatially-varying calibration model for the TEX₈₆ proxy. *Geochim. Cosmochim. Acta* 127, 83–106.
- Tierney, J.E., Tingley, M.P., 2015. A TEX₈₆ surface sediment database and extended Bayesian calibration. *Sci. Data* 2, 1–10.
- Varma, D., Hättig, K., Meer, M.T.J. Van Der and Reichart, G., 2023. Constraining water depth influence on organic paleotemperature proxies using sedimentary archives paleoceanography and paleoclimatology. 38. <https://doi.org/10.1029/2022PA004533>.
- Villanueva, L., Schouten, S., Sinninghe Damsté, J.S., 2015. Depth-related distribution of a key gene of the tetraether lipid biosynthetic pathway in marine Thaumarchaeota. *Environ. Microbiol.* 17, 3527–3539.
- Volkman, J.K., Eglinton, G., Corner, E.D.S., Forsberg, T.E.V., 1980. Long-chain alkenes and alkenones in the marine coccolithophorid *Emiliania huxleyi*. *Phytochemistry* 19, 2619–2622.
- Vorrath, M.E., Müller, J., Rebolledo, L., Cárdenas, P., Shi, X., Esper, O., Opel, T., Geibert, W., Munoz, P., Haas, C., Kuhn, G., Lange, C.B., Lohmann, G., Mollenhauer, G., 2020. Sea ice dynamics in the Bransfield Strait, Antarctic Peninsula, during the past 240 years: A multi-proxy intercomparison study. *Clim. past* 16, 2459–2483.
- Wagner, B., Benneke, O., Berg, S., Fritz, M., Klatt, O., Klug, M., Muhle, K., Ortlepp, S., Vogel, H. and White, D. 2008. Late Quaternary environmental history of the Rauer Group, as deduced from lake and marine basin sediments. H. Hubberten (Ed.), *Reports Polar Mar. Res.* 583, 80–95.
- Wei, B., Jia, G., Hefter, J., Kang, M., Park, E., Wang, S., Mollenhauer, G., 2020. Comparison of the U^K37, LDI, TEX₈₆^H, and RI-OH temperature proxies in sediments from the northern shelf of the South China Sea. *Biogeosciences* 17, 4489–4508.
- Weijers, J.W.H., Schouten, S., Spaargaren, O.C., Sinninghe Damsté, J.S., 2006. Occurrence and distribution of tetraether membrane lipids in soils: implications for the use of the TEX₈₆ proxy and the BIT index. *Org. Geochem.* 37, 1680–1693.
- Weijers, J.W.H., Lim, K.L.H., Aquilina, A., Sinninghe Damsté, J.S., Pancost, R.D., 2011. Biogeochemical controls on glycerol dialkyl glycerol tetraether lipid distributions in sediments characterized by diffusive methane flux. *Geochemistry, Geophys. Geosystems* 12, 1–15.
- Wu, J., Stein, R., Fahl, K., Syring, N., Nam, S., Il, H.J., Mollenhauer, G., Geibert, W., 2020. Deglacial to Holocene variability in surface water characteristics and major floods in the Beaufort Sea. *Commun. Earth Environ.* 1, 1–12.
- Wuchter, C., Schouten, S., Coolen, M.J.L., Sinninghe Damsté, J.S., 2004. Temperature-dependent variation in the distribution of tetraether membrane lipids of marine Crenarchaeota: Implications for TEX₈₆ paleothermometry. *Paleoceanography* 19, 1–10.
- Wuchter, C., Schouten, S., Wakeham, S.G., Sinninghe Damsté, J.S., 2005. Temporal and spatial variation in tetraether membrane lipids of marine Crenarchaeota in particulate organic matter: Implications for TEX₈₆ paleothermometry. *Paleoceanography* 20, 1–11.
- Xiao, W., Wang, Y., Zhou, S., Hu, L., Yang, H., Xu, Y., 2016. Ubiquitous production of branched glycerol dialkyl glycerol tetraethers (brGDGTs) in global marine environments: A new source indicator for brGDGTs. *Biogeosciences* 13, 5883–5894.
- Xiao, W., Xu, Y., Zhang, C., Lin, J., Wu, W., Xiaoxia, L., Tan, J., Zhang, X., Zheng, F., Song, X., Zhu, Y., Yang, Y., Zhang, H., Wenzhöfer, F., Rowden, A.A., Glud, R.N., 2023. Disentangling effects of sea surface temperature and water depth on hydroxylated isoprenoid GDGTs: insights from the hadal zone and global sediments. *Geophys. Res. Lett.* 50, 1–12.
- Yang, Y., Gao, C., Dang, X., Ruan, X., Lü, X., Xie, S., Li, X., Yao, Y., Yang, H., 2018. Assessing hydroxylated isoprenoid GDGTs as a paleothermometer for the tropical South China Sea. *Org. Geochem.* 115, 156–165.
- Yang, H., Xiao, W., Slowakiewicz, M., Ding, W., Ayari, A., Dang, X., Pei, H., 2019. Depth-dependent variation of archaeal ether lipids along soil and peat profiles from southern China: Implications for the use of isoprenoidal GDGTs as environmental tracers. *Org. Geochem.* 128, 42–56.
- Zell, C., Kim, J.H., Hollander, D., Lorenzoni, L., Baker, P., Silva, C.G., Nittrouer, C., Sinninghe Damsté, J.S., 2014. Sources and distributions of branched and isoprenoid tetraether lipids on the Amazon shelf and fan: Implications for the use of GDGT-based proxies in marine sediments. *Geochim. Cosmochim. Acta* 139, 293–312.
- Zeng, Z., Liu, X.-L., Farley, K.R., Wei, J.H., Metcalf, W.W., Summons, R.E., Welander, P. V., 2019. GDGT cyclization proteins identify the dominant archaeal sources of tetraether lipids in the ocean. *Proc. Natl. Acad. Sci. U. S. A.* 116, 22505–22511.
- Zhang, Y.G., Liu, X., 2018. Export Depth of the TEX₈₆ Signal. *Paleoceanogr. Paleoclimatology* 33, 666–671.
- Zhang, Y.G., Zhang, C.L., Liu, X.L., Li, L., Hinrichs, K.U., Noakes, J.E., 2011. Methane Index: A tetraether archaeal lipid biomarker indicator for detecting the instability of marine gas hydrates. *Earth Planet. Sci. Lett.* 307, 525–534.
- Zhu, C., Wakeham, S.G., Elling, F.J., Basse, A., Mollenhauer, G., Versteegh, G.J.M., Könneke, M., Hinrichs, K.U., 2016. Stratification of archaeal membrane lipids in the ocean and implications for adaptation and chemotaxonomy of planktonic archaea. *Environ. Microbiol.* 18, 4324–4336.
- Zweng M. M., Reagan J. R., Seidov D., Boyer T. P., Antonov J. I., Locarnini R. A., Garcia H. E., Mishonov A. V., Baranova O. K., Weathers K. W., Paver C. R. and Smolyar I. V. 2019. *World Ocean Atlas 2018, Volume 2: Salinity.*